final report

FEEDLOTS

Project code:	**B.FLT.0357**
Prepared by:	**Andrew Wiebe, Frank Quintarelli, Christine Killip Katestone Environmental Pty Ltd**
Date published:	**August 2010**
ISBN:	**9781741914696**

PUBLISHED BY
Meat & Livestock Australia Limited
Locked Bag 991
NORTH SYDNEY NSW 2059

Upgrade to the Feedlot Cattle Heat Load Forecast Service 2009-2010

Meat & Livestock Australia acknowledges the matching funds provided by the Australian Government to support the research and development detailed in this publication.

Abstract

The Feedlot Cattle Heat Load Forecast Service has been operational for 9 years, and has expanded to cover 91 locations across Australia, providing feedlot operators with warnings of impending adverse weather conditions that could lead to excessive heat loads for feedlot cattle.

Some limitations to the system have been identified by MLA and feedlot operators. These principally relate to poor performance at sites not located near a Bureau of Meteorology (BoM) Automatic Weather Station (AWS) site. The fact that the current system is limited to BoM AWS sites is inherent in its design. The use of statistical models was necessary during the original systems development to downscale the relevant meteorological parameters from model data supplied by the BoM.

To address this issue, a dynamical model was developed and performance testing was carried out on two test periods during the 2009-2010 summer. This initial developmental stage was undertaken to establish the dynamical models limitations and directions for improvement and to compare its performance against that of the current system. The results indicate that the dynamical model performs as well as the current system in predicting the HLI and associated meteorological parameters. While the current system is at the end of its development capacity the new system shows substantial scope for improvement.

Glossary

Term	Definition
AHLU	Accumulated heat load units
AFWA	US Air Force Weather Agency
AWS	Automatic weather station
BGT	Black globe temperature
BoM	Bureau of Meteorology
ECMWF	European Centre for Medium Range Weather Forecast
ENSO	El Nino/Southern Oscillation
exp	exponent
ºC	degrees Celsius
CSIRO	Commonwealth Scientific and Research Organization
FAA	Federal Aviation Administration (USA)
FSL	Forecast Systems Laboratory (USA)
GASP	Global Analysis and Prediction
GFS	Global Forecast System
hPa	Hectopascal
HLI	Heat Load Index
HPC	High performance computing
IOA	Index of agreement
km	kilometre
km/h	kilometre per hour
LAPS	Local area prediction system
LSM	Land surface model
m	metre
m/s	metres per second
m2	square metres
ME	Mean error
MLA	Meat and Livestock Association
NCAR	National Centre for Atmospheric Research (USA)
NCEP	National Centre for Environmental Prediction (USA)
NOAA	National Oceanic and Atmospheric Administration (USA)
NWP	Numerical Weather Prediction
pdf	Probability density function
RCOR	Pearson correlation coefficient
RMSE	Root mean square error
$RMSE_s$	Systematic root mean square error
$RMSE_u$	Unsystematic root mean square error
RH	Relative Humidity
Temp	Temperature
W	Watt
W/m^2	Watts per square metres
WRF	Weather Research and Forecasting model
WSpeed	Wind speed
SolRad	Solar radiation
3D	Three dimensional
%	percent
*	multiply
-	subtract
+	add
/	divide
=	equals

Executive summary

The Feedlot Cattle Heat Load Forecast Service has been operational for 9 years and has expanded to cover 91 locations across Australia. The service has been providing feedlot operators with warnings of impending adverse weather conditions that could lead to excessive heat loads for feedlot cattle. As the service progresses into its tenth year of operation some limitations to the system have been identified by MLA and feedlot operators, these were

- Reliability of daily upload of forecasts to the website has become an issue with the expansion of the forecasting to over ninety sites
- Poor performance at sites not located near a Bureau of Meteorology (BoM) Automatic Weather Station (AWS) site or located between two AWS sites giving conflicting forecasts
- AWS site locations not being representative of feedlot conditions

The first limitation was due to the web site being hosted by a third party. Forecast data had to be uploaded from Katestone Environmental before the forecast was made available to feedlot operators. As the number of sites progressively increased over time the amount of data being transferred became too large for the third party to process and the connection was lost. To address this issue Katestone Environmental will now be hosting the website in house on a dedicated web server attached to an onsite data store. The system will also be backed up offsite, meaning that even in the event of catastrophic failure of the Katestone server the forecast will still be available.

The fact that the current system is limited to BoM AWS sites is inherent in its design. The use of statistical models was necessary during the original systems development to downscale the relevant meteorological parameters from model data supplied by the BoM. These downscaled data then required training to determine the line of best fit for the multiple parameters, meaning that the data are then only representative of the location where the training data was measured and not where the actual feedlot is located, for which the forecast is intended.

Katestone Environmental developed a dynamical model capable of addressing this issue by simulating the environmental parameters used to calculate the HLI, for the entire Australian continent, on a low resolution grid with a resolution of 25 km and two high resolution grids at 9 km. These grids provide forecasts for any location in Australia to within 4.5 km for the high resolution grid and 12.5 km for the coarse grid.

During the 2009-2010 forecast season development of the dynamical model began and performance testing was carried out on two test periods. This initial developmental stage was undertaken to establish the dynamical models limitations and directions for improvement and to compare its performance against the current system. The results indicate that the dynamical model performs as well as the current system in predicting the HLI and associated meteorological parameters. While the current system is at the end of its development capacity the new system shows substantial scope for improvement.

Contents

1 Background

In the summer of 2001-02, Katestone Environmental undertook a feasibility study for MLA (FLOT.313) to develop a forecast for excessive heat load in feedlot cattle. This forecasting system utilised data from four feedlots that operated on-site meteorological stations and was based on the calculation of the Temperature Humidity Index (THI), previously developed as an indicator of human comfort.

Further studies on cattle heat stress (Gaughan et al. 2002) indicated that the Heat Load Index (HLI) was a better indicator of short-term cattle heat stress than the THI. From these studies it was also found that the Accumulated Heat Load Unit (AHLU), a parameter obtained by accumulating the number of hours the HLI exceeds a genus dependant threshold, is indicative of the long-term heat stress in feedlot cattle (see MLA report FLOT.327).

Since 2001-02 the Feedlot Cattle Heat Load Forecast Service has been expanded to include HLI and AHLU forecasts for 91 sites across Australia. The system has been operational for 9 years, providing feedlot operators with warnings of impending adverse weather conditions that could lead to excessive heat loads for feedlot cattle.

1.1 Current system

Forecasts of feedlot cattle heat load are based on the statistical downscaling of wind speed, temperature, relative humidity from Bureau of Meteorology (BoM) LAPS and GASP model data, at five levels above the surface ranging from 70 metres (m) to 1350 m, and BoM automatic weather station (AWS) data at 10 m above the surface for the 91 sites; and the derivation of solar radiation following Oke (1987).

These parameters are used to calculate the HLI (see Appendix A). A brief description of the calculation is provided below:

$$BGT = 1.33 * Temp - 2.65 * \sqrt{Temp} + 3.21 * \log(SolRad + 1) + 3.5$$

$$HLI_{LO} = 1.3 * BGT + 0.28 * RelHum - WSpeed + 10.66$$

$$HLI_{HI} = 1.55 * BGT + 0.38 * RelHum - 0.5 * WSpeed + \exp(2.4 - WSpeed) + 8.62$$

$$HLI = F * HLI_{HI} + (1 - F) * HLI_{LO}$$

Equation 1. Heat Load Index equations

where

Wspeed (Wind speed) is measured at the AWS in m/s.
Temp (Temperature) is measured at the AWS in ºC.
RelHum (Relative humidity) is expressed as a % and derived from measured AWS data.
SolRad (Solar radiation) is expressed in W/m² and derived following Oke (1987).
BGT (Black Globe Temperature) is derived from temperature solar radiation and expressed in ºC.
and
F = S(BGT, 25, 2.25)
Where
S(b, m, r) = 1 / (1 + exp(-X))

where

X = (b – m) / r
b = BGT value

m = middle of transition region (= 25 - the BGT value where HLIHI = HLILO)
r = rate at which the function switches from one extreme to the other (= 2.25).

The current system was developed when numerical weather prediction (NWP) across large regions was constrained by the availability of sufficient computational power, usually restricted to institutional users such as the CSIRO and the BoM, to provide a forecast of the environmental parameters required to calculate the HLI. As such it was out of necessity that the forecasting system was developed as a statistical model that interpolates the NWP and AWS data for a specific location.

These locations are typically airports where BoM has installed an AWS, the data from these sites are utilised primarily for climatology and aviation purposes and are often not representative of the climate experienced at any one particular feedlot. The physical distance between the forecast site and the feedlot that uses this forecast for management purposes ranges from 10's of kilometres (km) to 100's of km and can often be surrounded by very different terrain features, terrain types, elevations and aspects. The BoM AWS's also do not record solar radiation requiring the parameter to be calculated. This calculation does not account for cloud cover or aspect. The current system is not capable of accounting for the variations between AWS location and individual feedlot site characteristics. It is constrained by the availability of long-term data sets and the geographical resolution of the BoM AWS network and therefore cannot be improved or optimised further than its current capability

Moving into the 10th year of the Feedlot Cattle Heat Load Forecast Service an internal review of the current systems capabilities and limitations was undertaken by Katestone Environmental. The results of the review found that there are:

- **Limitations to adding in new locations -** Substantial historical database of synoptic and observational data are required to implement the forecasting models for a site, thus there is a lag of six to twelve months between the time that a request is made for forecasts and when forecasts are finally available.

- **Limitation to locations -** The forecasts are only representative for locations where BoM AWS sites are present and may not be representative of feedlot terrain, land use characteristics or micro-climate.

- **Limitation to frequency of delivery -** The forecast is only available once a day, when Bureau of Meteorology data becomes available usually by 7:30 am.

- **Limitation to delivery** – Data uploads to the website are constrained by the website operator's capacity to receive the data stream causing forecasts not to be updated for some locations and limiting the number of sites the current system can service in the future.

- **Limitation to improving model performance -** The existing forecast model has reached the end of its optimisation capacity and no further improvements are possible as any issues with the model cannot be resolved in the current configuration.

2 Project objectives

1. Investigate the options for improving the current forecasting service to overcome the limitations identified.

2. Evaluate the performance of a new forecasting service against the current system.

3. Recommend the most appropriate forecasting service for MLA taking into account the following:

    - o Robustness of system (delivery reliability)
    - o Ability to forecast HLI at feedlot locations
    - o Ease for future expansion of the system to new sites
    - o Ability to deliver the message in an uncomplicated manner to feedlot operators.

This report presents the project findings and compares the performance of the current system with the recommended new system based on numerical weather predictions. The performance is evaluated at 6 feedlot locations and 14 BoM AWS locations.

3 Proposed upgraded forecasting system

An upgraded forecasting system has been developed to address the issues outlined above. The core of the upgraded forecasting system is a NWP model, the Weather Research and Forecasting (WRF) model, which is the result of a collaborative partnership, principally among the National Centre for Atmospheric Research (NCAR), the National Oceanic and Atmospheric Administration (NOAA), the National Centers for Environmental Prediction (NCEP) and the Forecast Systems Laboratory (FSL), the US Air Force Weather Agency (AFWA), the Naval Research Laboratory, the University of Oklahoma, and the Federal Aviation Administration (FAA).

The WRF system forecasts solar radiation, temperature, relative humidity and wind speed adjusted for site specific characteristics of terrain and land use. The system consists of three model domains, one ‘mother’ domain covering all Australian states and territories at a horizontal resolution of 25 km and 28 vertical levels to 50 hPa and two high-resolution ‘daughter’ domains nested within the ‘mother’ domain at a horizontal resolution of 9 km. The daughter domains cover the south west corner of Western Australia and the majority of eastern Australia (Figure 2).

Forecasts at a resolution of 9 km means that any feedlot would be at most 4.5 km from the nearest forecast point, compared to the average distance of 45 km of the present system at the 6 feedlots assessed in this study (Appendix B). Also, as no historical databases are required, forecasts can be made available for a site within hours of the request being made. The only requirements on the part of the feedlot operators are to provide the latitude and longitude of the feedlot.

The WRF model consists of a three-dimensional (3D) atmosphere model coupled to a land surface model capable of calculating soil moisture content, surface run-off and evaporation. The atmosphere model and land surface model are fully coupled, meaning that feedback between surface characteristics and atmospheric conditions are fully resolved.

The WRF modelling system also contains advanced data assimilation features capable reading in real-time data from AWS, radar and satellite data streams for multiple locations. This feature has the potential to significantly improve short-term forecasts as the model's initial conditions are as close to reality as possible.

The system is highly configurable with multiple physics options and cumulus cloud options for calculating solar radiation, temperature, relative humidity and temperature for any location within the modelling domain to a maximum resolution of 9 km. The high degree of adjustment in the model means that site specific micro-climatological features can be tuned for a specific location either within the model run or in post-processing prior to delivery of the forecast.

The upgraded forecast system is run on a dedicated high performance computer (HPC) cluster developed by Katestone Environmental. The cluster handles the modelling and post-processing of forecast data before moving the data products to our onsite data store.

The forecast website will be hosted by Katestone Environmental, resolving any data transfer issues that may have occurred in the past as all data is processed, stored and accessed in house. The entire forecast system and website is backed up off site once a day, with a minimum turnaround time of 24 hours in case of a catastrophic failure of the system.

The proposed upgraded system will supply a new forecast every 12 hours (6 am and 6 pm) out to a maximum of three days. HLI forecasts will be provided at multiple resolutions covering the whole Australian continent as a colour shaded HLI contour (Figure 3). This type of display will enable quick and efficient assessments by feedlot managers of potential heat stress events over the next 6-7 days. The forecasts will be presented in a similar manner to the existing system for easy transition to the upgraded forecast system.

4 Methodology

4.1 Model Optimisation

To develop the upgraded forecasting system the size and resolution of the modelling domains needed to be optimised to ensure model run times remained within acceptable limits. High resolution domains were positioned to cover the largest number of current forecast locations and to encompass major terrain features, such as the Great Dividing Range of Southeast Queensland (Figure 2).

WRF has two options for generating terrain information, the United States Geologic Survey (USGS) 24-category data and the MODIS land cover classification of the International Geosphere-Biosphere Programme modified for the Noah Land Surface Model (LSM). Both options were used to initialise a series of two day test forecasts.

The WRF model showed improvements in temperature and relative humidity predictions with the LSM model using the MODIS land cover data. The LSM has a combined surface layer of vegetation and soil surface, over which surface energy fluxes are computed. The model has a total soil depth of two meters and uses gravitational free drainage at the model bottom as the lower boundary condition of soil moisture. This allows for the exchange of moisture between soil, vegetation and the atmosphere dynamically during each model time step, meaning that the effects of rainfall on the surface are accounted for. The Noah LSM has been shown to improve operational mesoscale analysis and forecasting (Ek et al., 2003) and has been used here.

To assess the performance of the upgraded forecasting system two one week periods were chosen from the 2009-2010 forecast period. These periods were chosen as they showed a wide range of HLI values (high and low) and coincided with available on site data from MLA feedlots. The periods were:

- February 9 to 17 2010
- March 2 to 10 2010

The forecasts for 14 BoM AWS sites covering the states of Queensland, NSW, Victoria, South Australia, Western Australia and Tasmania (Figure 1) and six MLA feedlot sites were assessed using statistical measures of forecast accuracy and model variability (Appendix C).

As the WRF model is highly configurable a sensitivity test was conducted to determine the bias, or degree of error, in the model forecasts. The results of the sensitivity test will guide the optimisation of the models algorithms and fine tuning for site specific micro-climates (Appendix D).

5 Results and discussion

For ease in presentation and analysis of the two forecasting systems the current system is called KAT and the upgraded system is called WFR. All statistical measures used in this report are explained in Appendix C.

5.1 BoM AWS

The upgraded forecast system performed well in predicting the HLI at the 14 BoM AWS sites (Table 1). The WRF model forecasts showed good skill in predicting the variability and the magnitude of the HLI at these sites (IO A > 0.9 and RCOR > 0.8), while both models tend to under predict the HLI by similar magnitudes (Figure 3).

Table 1 Performance statistics of WRF predicted Heat Load Index

Parameter	intercept	slope	r^2	RMSE	$RMSE_s$	$RMSE_u$	IOA	RCOR	ME
Emerald	12.25	0.82	0.84	5.56	2.94	4.72	0.95	0.92	-1.70
Mareeba	5.93	0.88	0.78	7.23	3.72	6.19	0.93	0.88	-3.34
Oakey	2.51	0.92	0.85	5.66	3.08	4.75	0.95	0.92	-2.91
Deniliquin	4.53	0.93	0.82	5.95	0.97	5.87	0.95	0.90	-0.05
Griffith	7.34	0.86	0.78	6.86	2.83	6.25	0.93	0.88	-2.12
St George	-4.15	1.00	0.76	7.88	4.31	6.59	0.90	0.87	-4.31
Tamworth	0.70	0.90	0.88	7.75	6.10	4.78	0.93	0.94	-5.94
Charlton	3.39	0.92	0.74	7.26	2.31	6.88	0.92	0.86	-2.05
Katanning	10.77	0.83	0.67	6.85	2.00	6.55	0.90	0.82	0.32
Southern Cross	5.76	0.90	0.71	7.05	1.54	6.88	0.92	0.85	-0.87
Morawa	5.07	0.90	0.67	8.00	1.91	7.77	0.90	0.82	-1.44
Minipa	6.19	0.92	0.85	4.84	1.64	4.55	0.96	0.92	1.36
Port Augusta	9.30	0.85	0.84	5.21	2.01	4.80	0.95	0.91	-0.44
Warra	9.59	0.83	0.81	4.23	1.65	3.90	0.95	0.90	-0.15

The upgraded system also performs well in predicting the meteorological parameters used in the HLI calculation. The model showed very good skill in predicting the temperature with an average IOA of 0.95 and RCOR of 0.92. The average RMSE was 2.3 across all sites compared to 2.0 for the current system (Appendix E).

The model performed well for predictions of relative humidity showing good skill (average IOA of 0.85 and RCOR of 0.79). The average RMSE was 15 across all sites compared to 11 for the current system. Predictions for wind speed did not perform as well as the other parameters with an average IOA of 0.7 and RCOR of 0.54, although the average RMSE was 2 compared to 2.8 for the current system (Appendix E).

The results indicate that the upgraded system performs as well as the current system at BoM AWS sites (Appendix E).

5.2 MLA feedlots

Onsite meteorological data was provided from six MLA feedlots for the forecast test period. Forecasts from the current system and the upgraded system were compared to the meteorological parameters measured onsite at the feedlots and the calculated HLI. The results for Feedlot 1 and Feedlot 4 are presented below. Results for all six sites are presented in Appendix F.

5.2.1 Feedlot 1

The one day ahead forecast for the existing system (KAT) and the upgraded system (WRF) were compared with the onsite meteorological data recorded at Feedlot 1 feedlot for the two test periods. Figure 4 shows the time series of the two forecasts and the actual HLI calculated for the test periods. Both KAT and WRF show good correlation (RCOR) with the actual HLI (0.98) and similar root mean square errors (RMSE ≈3.5) with low mean errors (ME) (< 1) (Table 1). Regression analysis indicates that both systems perform very well with r2 values greater than 0.9 and residual errors predominantly less than 5 HLI units with some outliers indicating over and under predictions of 10 (WRF) to 15 (KAT) units (Figure 5).

Both systems showed good performance in predicting the temperature and relative humidity with good correlations ≈ 0.9. Both systems tended to under predict the temperature on average by 1 °C (Table 1 ME). Relative humidity showed good agreement with the onsite data, however the error was slightly higher than for temperature but of the same magnitude for both systems. WRF tended to under predict the wind speed by 1.3 m/s while KAT over predicted by 2.5 m/s. WRF showed a higher systematic error ($RMSE_s$) meaning that the majority of the error is due to model bias and not random fluctuations in the data defined by the unsystematic error ($RMSE_u$).

Table 2 Summary statistics for forecasting performance at Feedlot 1

Parameter	intercept	slope	r^2	RMSE	$RMSE_s$	$RMSE_u$	IOA	RCOR	ME
WRF HLI	0.19	1.01	0.93	3.31	0.62	3.25	0.98	0.97	0.62
KAT HLI	4.52	0.93	0.92	3.46	0.84	3.35	0.98	0.96	0.25
WRF Temperature (°C)	4.56	0.75	0.86	2.03	1.55	1.31	0.93	0.93	-1.15
KAT Temperature (°C)	6.49	0.71	0.82	1.88	1.27	1.38	0.94	0.91	-0.27
WRF Relative Humidity (%)	28.77	0.68	0.79	12.17	9.19	7.98	0.91	0.89	5.65
KAT Relative Humidity (%)	31.80	0.65	0.79	12.79	10.32	7.56	0.89	0.89	6.65
WRF Wind speed (m/s)	2.50	0.47	0.43	3.07	2.35	1.97	0.76	0.66	-1.30
KAT Wind speed (m/s)	0.15	1.33	0.63	4.67	2.79	3.74	0.77	0.80	2.51

5.2.2 Feedlot 4

The one day ahead forecast for the existing system (KAT) and the upgraded system (WRF) were compared with the onsite meteorological data recorded at Feedlot 4 for the two test periods. Figure 6 shows the time series of the two forecasts and the actual HLI calculated for the test periods. Both KAT and WRF show good correlation (RCOR) with the actual HLI (WRF = 0.96 and KAT = 0.94) (Table 2). WRF is shown to perform better than KAT with a ME of 0.00 and RMSE of 3.74 compared to a ME of -1.6 and RMSE of 5.51 for KAT.

Regression analysis indicates that both systems perform very well with r2 values greater than 0.92 (WRF) and 0.86 (KAT), however KAT does show a wider spread of errors than WRF (Figure 7). Both systems showed generally good performance in predicting the temperature and relative humidity with WRF slightly edging out KAT. Overall WRF showed better skill in predicting the meteorological parameters with less error than KAT.

Table 3 Summary statistics for forecasting performance at Feedlot 4

Parameter	Intercept	Slope	r^2	RMSE	$RMSE_s$	$RMSE_u$	IOA	RCOR	ME
WRF HLI	-0.41	1.01	0.93	3.74	0.08	3.74	0.98	0.96	0.00
KAT HLI	-5.55	1.06	0.88	5.51	1.79	5.21	0.96	0.94	-1.60
WRF Temperature (°C)	5.36	0.80	0.82	2.23	1.20	1.88	0.94	0.90	0.65
KAT Temperature (°C)	2.94	0.89	0.71	2.89	0.71	2.80	0.92	0.85	0.47
WRF Relative Humidity (%)	20.62	0.65	0.60	13.45	7.46	11.19	0.87	0.77	0.25
KAT Relative Humidity (%)	26.29	0.64	0.55	15.46	9.45	12.23	0.84	0.74	5.71
WRF Wind speed (m/s)	2.51	0.60	0.15	2.27	1.59	1.62	0.51	0.39	1.52
KAT Wind speed (m/s)	4.69	1.14	0.22	5.59	5.03	2.44	0.28	0.47	5.03

5.3 Discussion

Further analysis of the onsite meteorological data revealed some discrepancies with the calculated HLI, namely the measured relative humidity which is seen to exceed 100% on several occasions at most of the sites. This may cause the HLI calculation to be higher than is realistically possible. Analysis of the data and determination of the calibration measures used for the various data loggers is required to address this issue.

Concerning the predicted meteorological parameters both systems show a similar distribution of systematic and unsystematic errors. Unsystematic errors are due to random fluctuations in the data set and therefore cannot be predicted or easily corrected. Systematic errors on the other hand are not random but are an artefact of the models algorithms. As such they can be corrected by altering the models configuration. Both errors, systematic and unsystematic, are sensitive to initial conditions, where the magnitude of the error can be reduced if real time data of the current condition is available to initialise the forecast.

Both systems show errors in the prediction of relative humidity of ± 10 – 15% which can introduce an error of roughly 4 units to the HLI calculation. The error in the temperature prediction is generally within ± 1 °C and wind speed is ± 2 – 3 m/s. The relative contribution of these errors to the HLI calculation is on average less than for relative humidity, approximately 2 HLI units. However, the magnitude of the error in the HLI calculation (Appendix D) is larger at low wind speeds or high temperatures.

The ability to correct the inherent bias towards under predicting the HLI in the forecast system is possible using the WRF model, where model algorithms and physics options can be altered or corrections applied in post-processing, this is a technique known as ‘bias correction’. The current system does not have to capacity to apply any of these changes or account for variations in the forecast parameters such as rainfall or solar radiation.

The LSM module in the WRF system adjusts the soil moisture content dynamically as the forecast progresses, thereby accounting for rainfall and the variations in relative humidity. However when the forecast is restarted every 12 hours the build up and drainage of moisture in the soil is restarted from zero, this is known as a ‘cold start’. Conversely a ‘hot start’ will use the previous forecast as an initialisation filter to dynamically allocate the initial conditions in the model then adjust the boundary conditions for the updated global forecast. Along with the assimilation of BoM data from regionally representative locations the forecast of temperature and relative humidity can be significantly improved in the WRF system.

The results indicate that the upgraded system performs as well as the current system at the feedlot sites assessed and outperforms the current system at some of them (Appendix F).

6 Success in achieving objectives

To improve the current Feedlot Cattle Forecasting Service the underlying computer model that generates the forecast needed to move from a statistical model to a dynamical model. To achieve this objective Katestone Environmental investigated several next generation mesoscale numerical weather prediction systems, capable of forecasting the environmental variables required for calculating the HLI at a high resolution across Australia.

The Weather Research and Forecasting (WRF) model was chosen for its high level of configurability and optimisation potential. WRF is a research and operational grade weather prediction system that has been extensively validated (Skamarock et al. 2004 and Michalakes et al. 2005) and is currently used by many national weather service’s around the world. WRF is a community model, meaning that the source code is freely available for use and modification. This is a key factor in the choice of a dynamical model suitable for the forecast service, where time, resolution and interaction of key parameters needs to be finetuned for a particular location.

The performance of the WRF system was evaluated for two forecast periods during the 2009-2010 forecast season. The impetus to the evaluation was two-fold:

1. Evaluate the performance of the model against the current system in forecasting the HLI at BoM AWS sites and at feedlots where hourly onsite data was available.

2. Determine the bias inherent in the model for bias correction and optimisation.

The results show that the WRF system performs as well as, and at times outperforms, the current the system in forecasting the HLI and the biases in the WRF system are of the same magnitude as the current system. This indicates that the WRF can significantly improve the HLI forecast through optimisation of algorithms and model resolution and through bias correction techniques as the system already performs well with minimal finetuning.

An upgraded forecasting system has been developed to address the limitations apparent in the current heat load forecasting service. The upgraded system will be wholly operated and maintained by Katestone Environmental, negating any downtime of the forecast or failure to deliver due to third party web hosting and data dropout during transfer.

The use of a state of the science weather forecasting model (WRF) allows the forecast to be generated dynamically instead of statistically for any location in Australia. The system will no longer require 3-6 months of lead time to train the model to forecast for additional sites. New sites can be added in a matter of hours and forecasts posted on the website within 2-3 days.

High resolution modelling domains increase the proximity of forecast points to within 4.5 km of any feedlot within that domain. Maximum distance of any feedlot in Australia to a forecast point will be 12.5 km compared to the current system which can range from 10's of km to 100's km. The high resolution of the forecast takes into account the differences in terrain features and terrain types between feedlot sites and BoM AWS sites. The need to interpolate between several sites that are not representative of a feedlot location will no longer be required.

Forecasts will be provided twice daily at 6 am and 6 pm. The forecast data will be displayed in a similar way to the current system with the added feature of a 6-7 day HLI contour map covering all Australian states and territories.

The upgraded system performs as well as the current system in predicting the meteorological variables used to calculate the HLI. The upgraded system has the scope to significantly improve on the current systems ability to accurately forecast the HLI at the location of MLA feedlots. High resolution terrain, data assimilation and dynamic integration of the moisture exchanges between soil and vegetation allow the system to simulate the micro-climate of individual feedlot locations.

7 Impact on Meat & Livestock Industry – Now and in 5 years time

7.1 Now

The upgraded system will improve the management of feedlot cattle by providing site specific forecast of impending adverse weather conditions that could lead to excessive heat loads for feedlot cattle. The current version of the forecasting service is constrained to the BoM AWS monitoring network and is not representative of individual feedlot terrain features, types, aspects or elevations, meaning that feedlot operators were required to interpolate for themselves between several sites or even look at the wrong site altogether. The upgraded system solves this problem by generating a forecast within 4.5 km of most feedlots to a maximum distance of 12.5 km. The upgraded system also accounts for rainfall and soil moisture levels, which can have a significant impact on the ground level temperature and relative humidity.

The upgraded system will provide forecasts twice daily (6 am and 6 pm) to give feedlot operators the most up to date information on which they can base daily operational management decisions. The Australian wide forecast contour map will provide operators with a complete picture of the HLI across Australia for easy identification of adverse conditions or potential hot spots over the coming week.

Under the upgraded system there is no downtime between requests for forecasts at a new location and the delivery of the forecast. By simply providing the feedlots latitude and longitude the forecast can be extracted from the model and posted on the website.

7.2 5 Years

The development of the forecasting system is a continual process. As computing power increases so does the capability of the system to increase the resolution of the forecast and improve its accuracy. As the model is run over the entire Australian continent data for any location can be extracted and a forecast provided. The system also provides the potential to improve the characterisation of the terrain type, actually accounting for the surface energy exchanges that occur at the feedlot.

By moving to a dynamical model to forecast the HLI, an historical database can be developed where specific high heat load events and their causes can be analysed and defined. The results of this analysis can be applied to long-term data sets generating climatology of heat stress for specific regions, and cattle breeds under various conditions.

The data generated will also allow investigations into the potential for seasonal forecast of the HLI accounting for the El Nino/Southern Oscillation (ENSO) index and the potential changes to HLI climatology due to climate change.

8 Conclusions and recommendations

The WRF system performs as well and at times better than the existing system. The advantages of the WRF system are that further optimisation of the forecast for site specific conditions and the assimilation of real-time data is possible. The WRF system comes with improved data delivery from Katestone Environmental's dedicated HPC cluster and data storage unit and is available for a greater number of sites (unlimited number of locations compared to only AWS sites for current system).

Forecast delivery is increased to twice daily and covers the entire Australian continent. The display of forecast data will remain similar to previous forecast years with an added colour shaded contour for quick regional assessment and 6-7 day planning. The WRF system will allow for greater flexibility of data delivery improving the efficiency and level of service to MLA registered feedlots.

New sites can be added within a few days of the request, compared to 6 to 12 months under the existing system. Historical data bases of HLI forecasts can now be stored for re-analysis of forecast performance and to generate HLI climatologies, which may extend the 6-7 day forecast out to months or next season forecasts based on the Southern Oscillation Index.

The system can also be tested using different initial global forecasts. The version tested here relied on the Global Forecast System (GFS) administered by NOAA out of the United States. WRF can also be initialised with the European Centre for Medium Range Weather Forecast (ECMWF) global ensemble or the Australian Bureau of Meteorology LAPS model. The ECMWF and LAPS are available commercially while the GFS is publicly available making it ideal for testing and model configuration.

Katestone Environmental recommends progressing with the WRF forecast system, for its flexibility in configuration and delivery of timely heat load forecasts. The model is highly configurable and by investigating the models inherent biases and correcting for site specific micro-climates the system can significantly improve the accuracy of heat load forecasts for feedlot cattle for any location in Australia.

9 Bibliography

Ek, M. B., K. E. Mitchell, Y. Lin, E. Rogers, P. Grunmann, V. Koren, G. Gayno, and J. D. Tarpley (2003), Implementation of Noah land surface model advancements in the National Centers for Environmental Prediction operational mesoscale Eta model, J. Geophys. Res., 108(D22), 8851, doi:10.1029/2002JD003296, 2003.

Gaughan, J. Goopy J. and Spark J (2002), "Excessive Heat Load Index for Feedlot Cattle", University of Queensland.

Michalakes, J., J. Dudhia, D. Gill, T. Henderson, J. Klemp, W. Skamarock, and W. Wang: The Weather Research and Forecast Model: Software Architecture and Performance. Proceedings of the Eleventh ECMWF Workshop on the Use of High Performance Computing in Meteorology. Eds. Walter Zwieflhofer and George Mozdzynski. World Scientific, 2005, pp 156 – 168.

Oke TR (1987), "Boundary Layer Climates", Second Edition, Routledge.

Skamarock, W. C., 2004: Evaluating Mesoscale NWP Models Using Kinetic Energy Spectra. Mon. Wea., Rev., 132, 3019-3032.

Figure 1 Current coverage of Feedlot Cattle Heat Load Forecast Service

Location: Australia	Data source: Google Earth and Bureau of Meteorology AWS locations	Units: n/a
Type: Google Earth Image	Prepared by: Andrew Wiebe	Date: July 2010

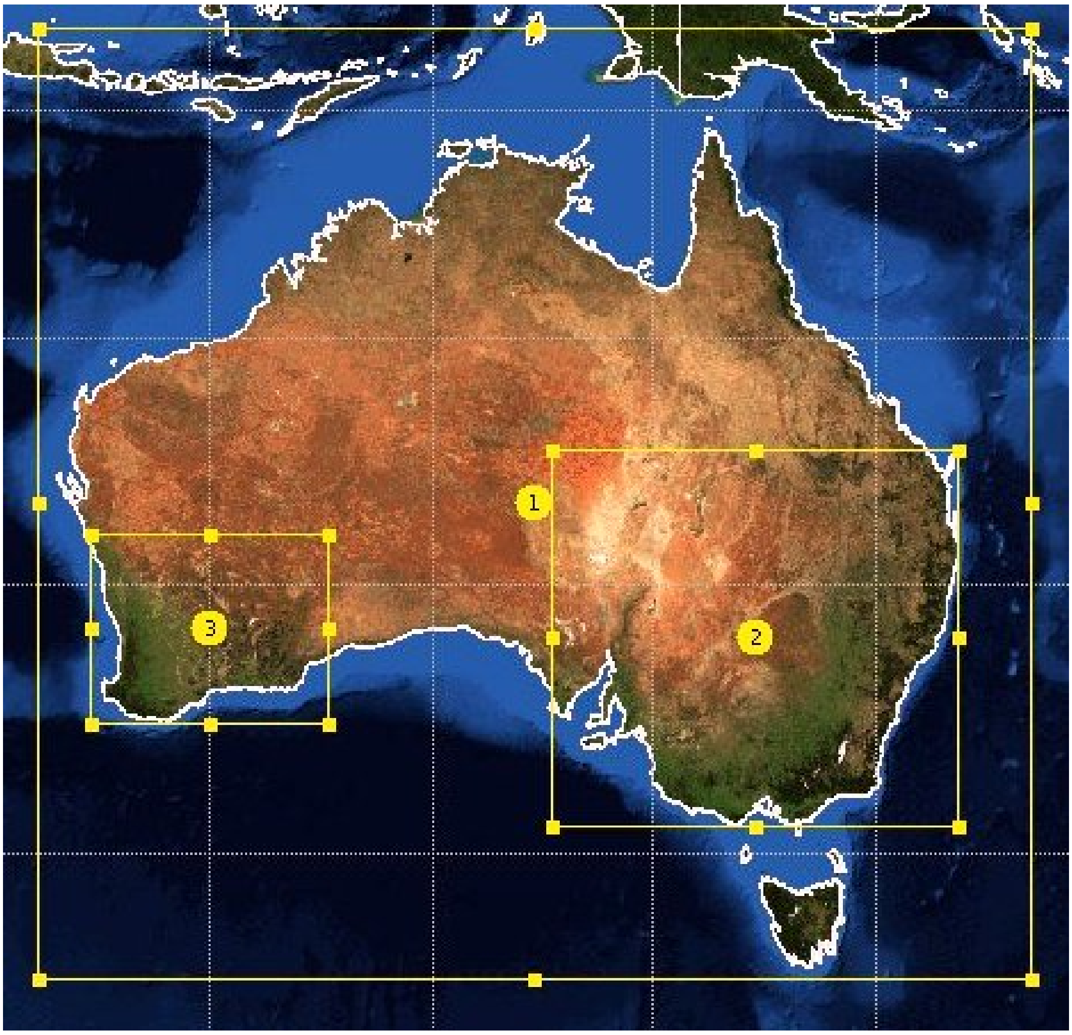

Figure 2 WRF model domain

Location: Australia	Data source: WRF-Portal Domain Wizard	Units: n/a
Type: WRF computational domain	Prepared by: Andrew Wiebe	Date: July 2010

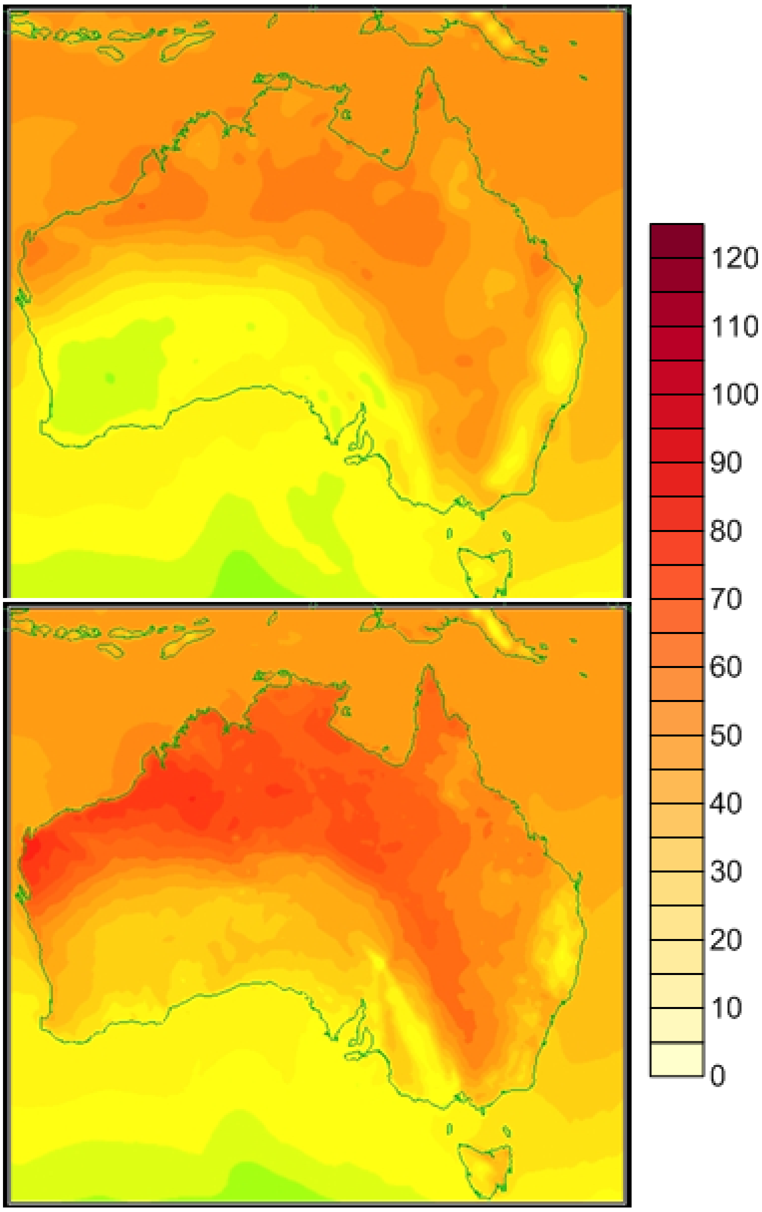

Figure 3 Example of two day ahead Australia wide Heat Load Index (HLI) forecast

Location: Australia	Data source: WRF MLA forecast	Units: HLI
Type: Colour shaded contour	Prepared by: Andrew Wiebe	Date: July 2010

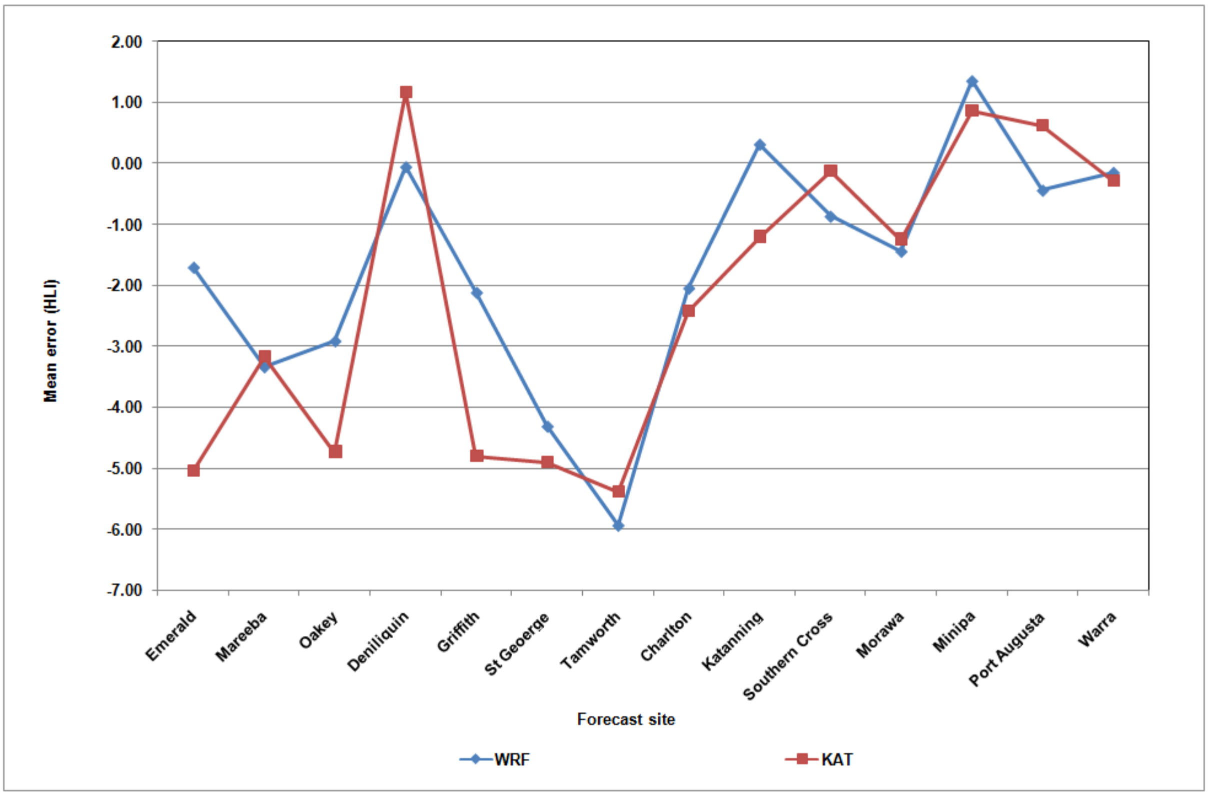

Figure 4	Mean error WRF and KAT Heat Load Index (HLI) forecast

Location: Australia	Data source: WRF MLA forecast	Units: HLI
Type: Colour shaded contour	Prepared by: Andrew Wiebe	Date: July 2010

a) February Forecast

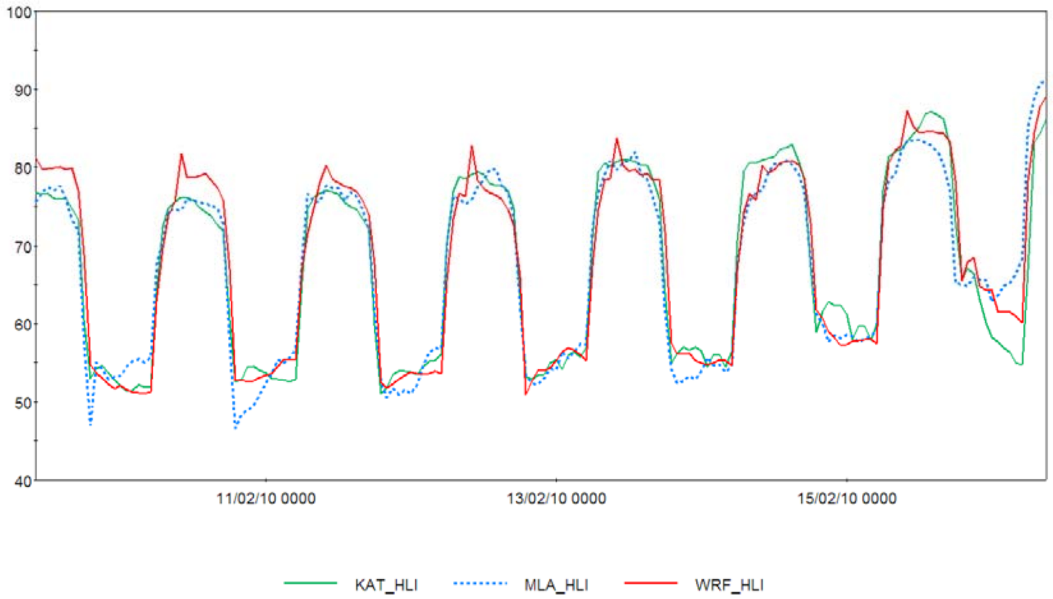

b) March Forecast

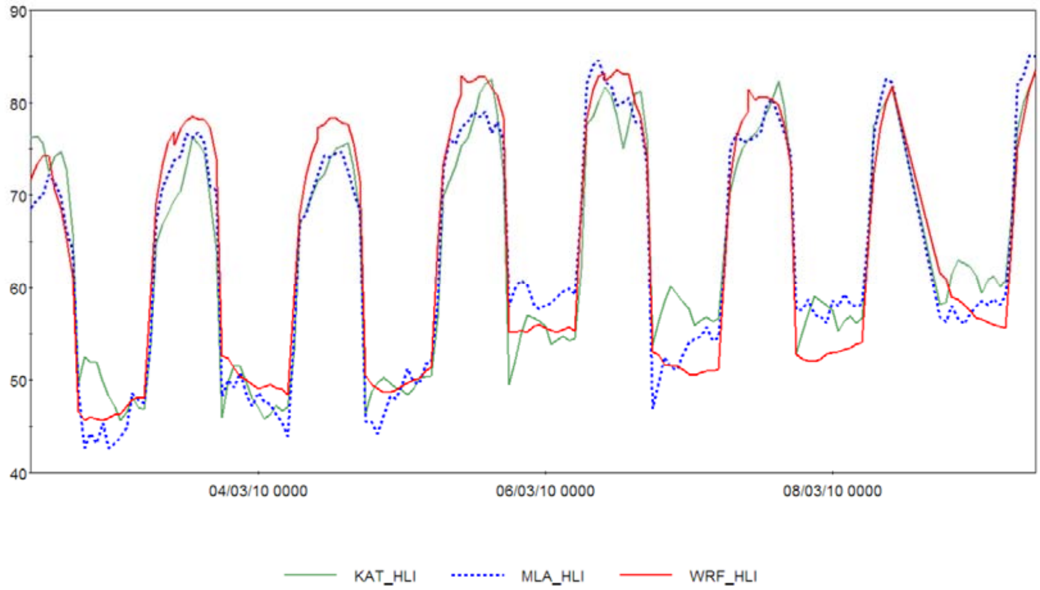

Figure 5 Heat Load Index (HLI) at Feedlot 1 calculated by MLA, KAT and WRF for the forecast assessment periods

Location: Feedlot 1	Data source: Feedlot 1 on site meteorology (MLA), WRF and KAT forecast	Units: HLI
Type: Time series	Prepared by: Andrew Vernon	Date: July 2010

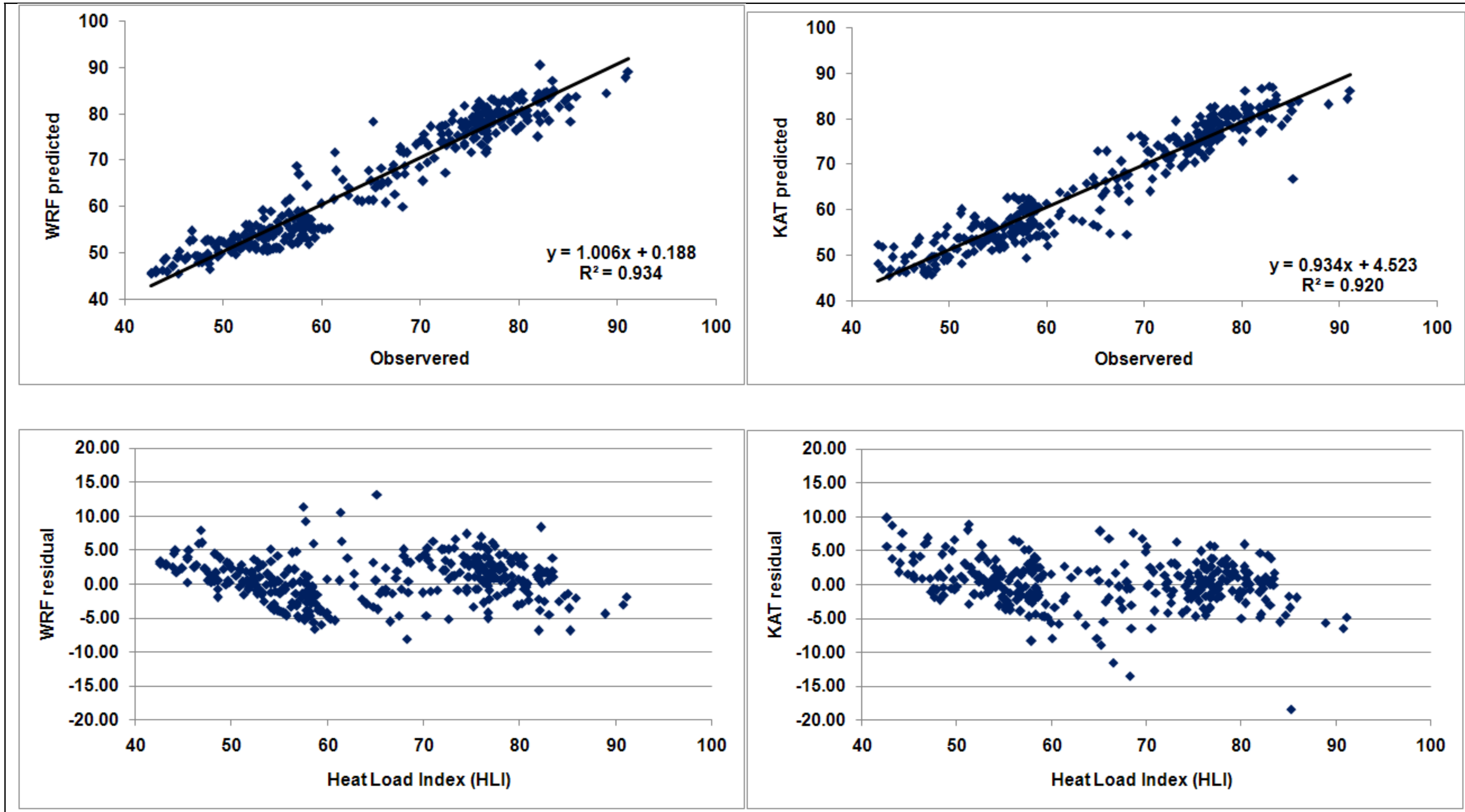

Figure 6 Regression and residual plots of HLI from KAT and WRF predictions at Feedlot 1

Type:	Data source:	Prepared by:	Date:
Regression and residuals charts	WRF and KAT	Andrew Vernon	July 2010

a) February Forecast

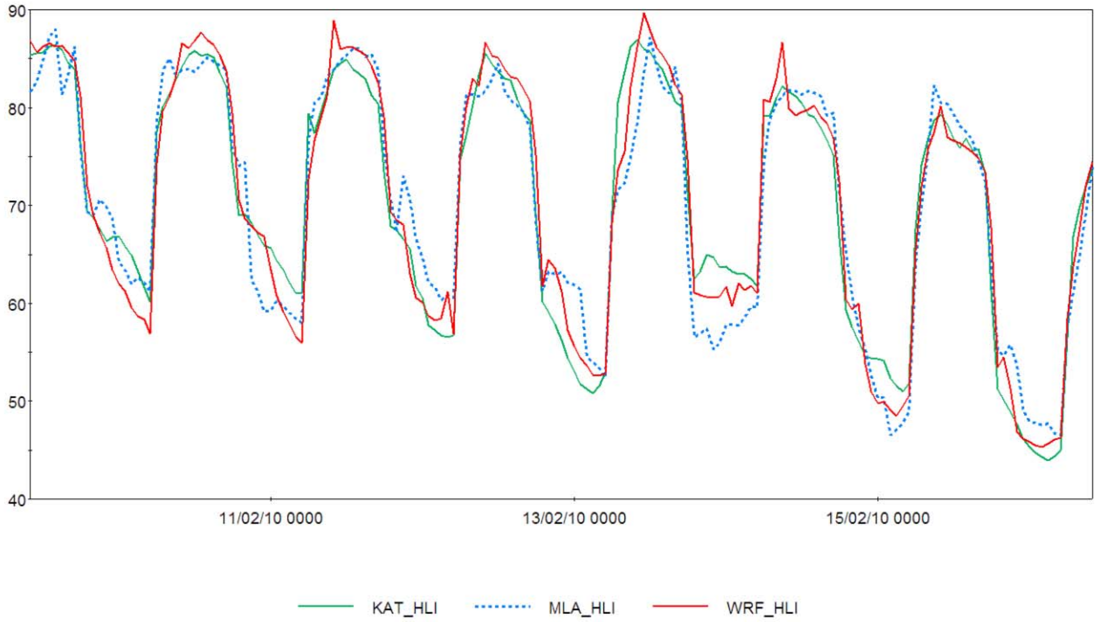

b) March Forecast

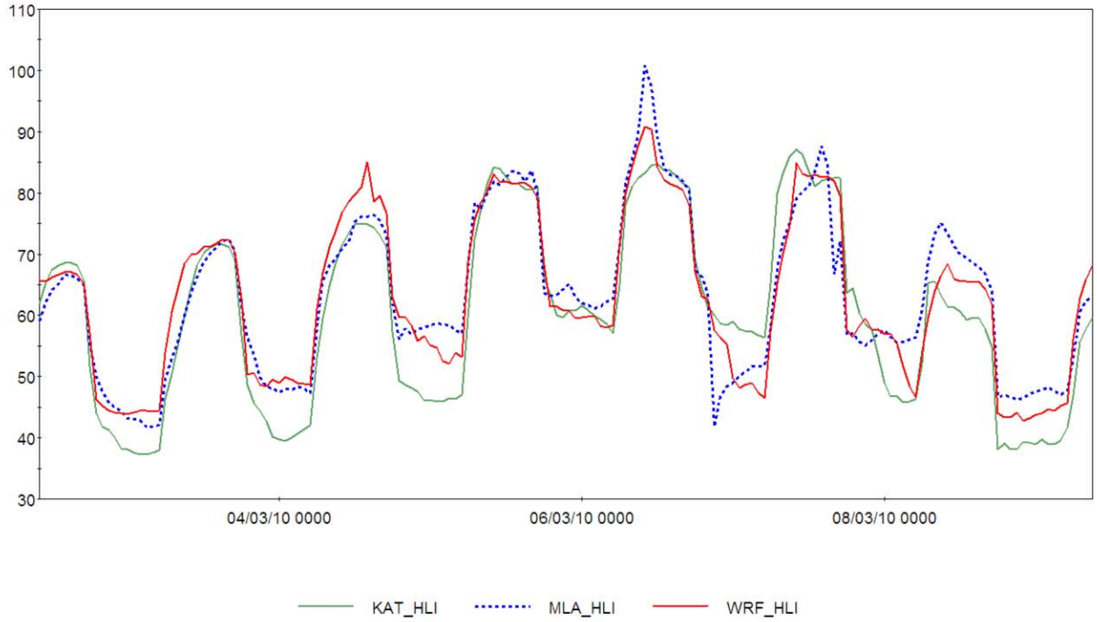

Figure 7	Heat Load Index (HLI) at Feedlot 4 calculated by MLA, KAT and WRF for the forecast assessment periods	
Location: Feedlot 4	Data source: Feedlot 4 on site meteorology (MLA), WRF and KAT forecast	Units: HLI
Type: Time series	Prepared by: Andrew Vernon	Date: July 2010

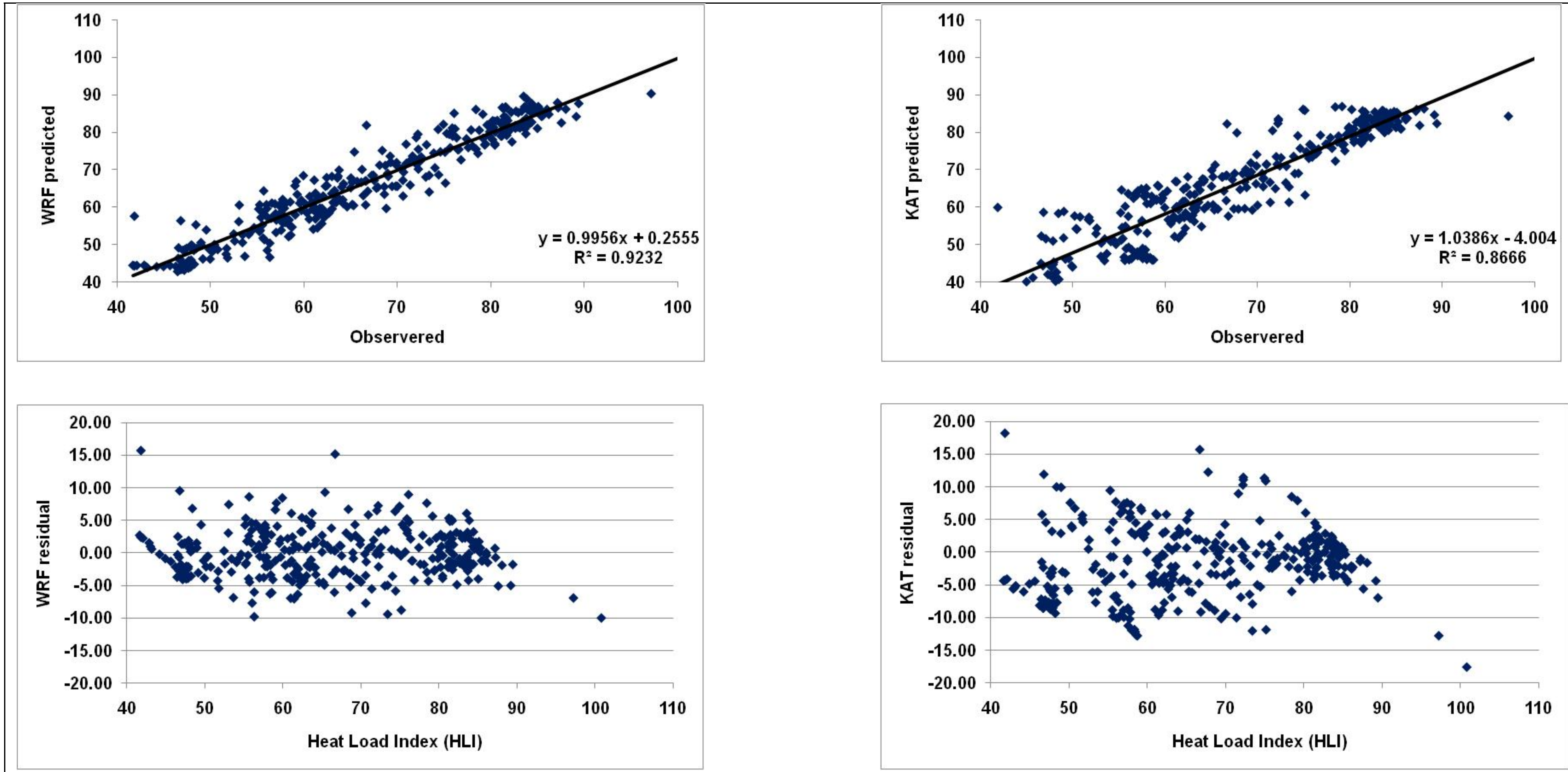

Figure 8 Regression and residual plots of HLI from KAT and WRF predictions at Feedlot 4

Type:	Data source:	Prepared by:	Date:
Regression and residuals charts	WRF and KAT	Andrew Vernon	July 2010

10 Appendices

10.1 Appendix A

A1 Method for calculating HLI

A1.1 Introduction

In the preceding text it was reported that errors in the AHLU forecasts arise from two sources – errors introduced by the technique used in calculating the AHLU and errors in the (forecast) HLI. Any disagreement between the observed and forecast HLI can in turn be attributed to errors in the forecasts and errors introduced by the method used to calculate the HLI. Inspection of the graphs of forecast HLI plotted against observed HLI indicates that the performance of the forecasting technique can be considered satisfactory. Comparison of the HLI graphs to the corresponding AHLU graphs reveals that (a) the AHLU graphs show much greater scatter and (b) given that the AHLU is dependent only on the HLI, one might expect the AHLU forecast performance to be similar to the HLI forecast performance.

There is limited scope for improving the quality of the forecasts as these depend on the accuracy of forecasts provided by the Bureau of Meteorology. The other option is to investigate the errors caused by the technique used to calculate the HLI. The aim of this section is to develop alternative method for determining the HLI and AHLU.

A1.2 Discrepancies caused by the calculation technique

Recall that two expressions are used to determine the HLI – dependent on the BGT being above or below 25. To calculate the HLI for each data record, the following equations were used:

$$BGT = 1.33*Temp - 2.65*\sqrt{Temp} + 3.21*\log(SolRad + 1) + 3.5$$

$$if \;\; BGT < 25$$

$$HLI = 1.3*BGT + 0.28*RelHum - WSpeed + 10.66$$

$$else$$

$$HLI = 1.55*BGT + 0.38*RelHum - 0.5*WSpeed + \exp(2.4 - WSpeed) + 8.62$$

Equation A1. Heat Load Index equations

where

Wspeed (Wind speed) is measured in m/s.
Temp (Temperature) is measured in ºC .
RelHum (Relative humidity) is expressed as a %.
SolRad (Solar radiation) is measured in W/m²
BGT (Black Globe Temperature) stated in ºC.

To illustrate the discrepancy caused by this technique, assume the following (purposely chosen) values for the observed and forecast parameters:

- Forecast and observed relative humidity = 70%
- Forecast and observed wind speed = 2 m/s
- Solar radiation = 500 W/m2
- Forecast temperature = 18.0 ºC ; Observed temperature = 18.2 ºC

Note that all parameters are equal except for the temperatures which differ by 0.2 ºC. For this set of parameters, one would expect the resulting BGTs and the HLIs to be almost equal. Using Equation A1, we find that the forecast and observed BGTs are 24.9 ºC and 25.1 ºC respectively – which are almost equal as expected. However, since the forecast BGT value is below the 25 ºC threshold and the observed BGT value is above the threshold, two different equations are used to determine the HLI. The values thus obtained are 60.6 for the forecast and 74.6 for the observed HLI value – a jump of 14 HLI units. In the example just given, the HLI values are below the lower Thermo-Neutral threshold (77), corresponding to conditions where cattle might be recovering from a previous heat episode. However, the discrepancy in HLI values results in a significant difference in recovery rates between the observed and predicted AHLU values.

To further illustrate this, the forecast HLI values for Amberley plotted against the observed HLI values are shown in Figure A1. Noteworthy features include the majority of data points being grouped into two distinct elongated clusters aligned along the line of unity slope and two sets of lightly populated outliers, labelled "A" in the figure, that represent instances where the two different expressions were used to calculate the HLI. The sharp cut-off at HLI = 50 has not been applied to these data.

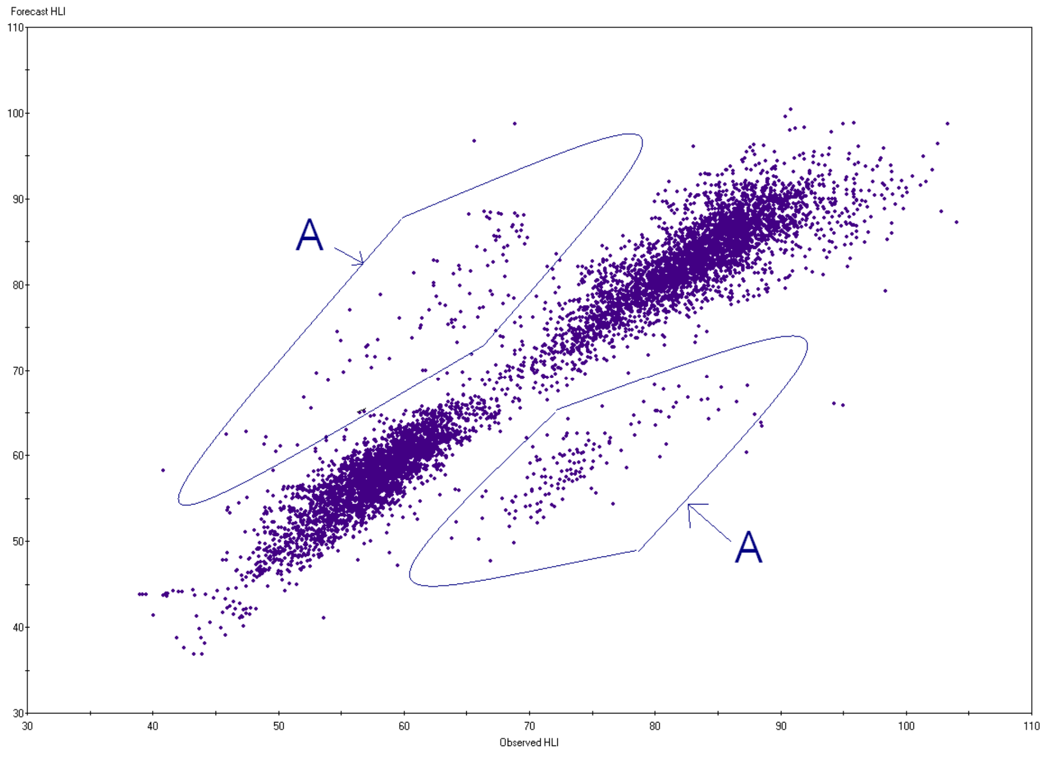

Figure A1: Forecast HLI plotted against Observed HLI. Equation A1 was used to calculate these HLI values.

A1.3 Brief overview of an alternative method for calculating the HLI

From the preceding discussion, it is evident that an improvement in the forecasts may be possible by making the transition between the two HLI expressions more gradual instead of the sharp step function currently used. To achieve this, a weighting function based on the sigmoid function commonly used for a similar purpose in artificial neural networks has been adapted for this investigation. The form of this function is:

S(b, m, r) = 1 / (1 + exp(-X))

Where

X = (b – m) / r
b = BGT value
m = middle of transition region (= 25)
r = rate at which the function switches from one extreme to the other (= 2.25).

The final HLI value is obtained by computing a linear combination of HLI values as follows:

HLI = F * HLIHI + (1 – F) * HLILO

Where

F = S(BGT, 25, 2.25)
HLIHI = HLI value determined using the expression for BGT >= 25
HLILO = HLI value determined using the expression for BGT < 25

A plot of this function is shown in Figure A2. The value of this function is 0.5, or 50%, for a BGT of 25, resulting in equal contributions from each HLI expression at the BGT value where calculation of HLI switches between the two expressions. This midpoint value is set by the "m" parameter. The value of the rate parameter "r" (= 2.25) was chosen so that for a BGT value of 20, the HLI value consisted of 10% HLIHI and 90% HLILO, with the reverse combination for a BGT value of 30. Note that for this example, the value of "r" (2.25) and the 10% and 90% function values were arbitrarily chosen. The effects of varying "r" will be discussed in the next section. The intention of this section is only to introduce the method and illustrate what can be achieved.

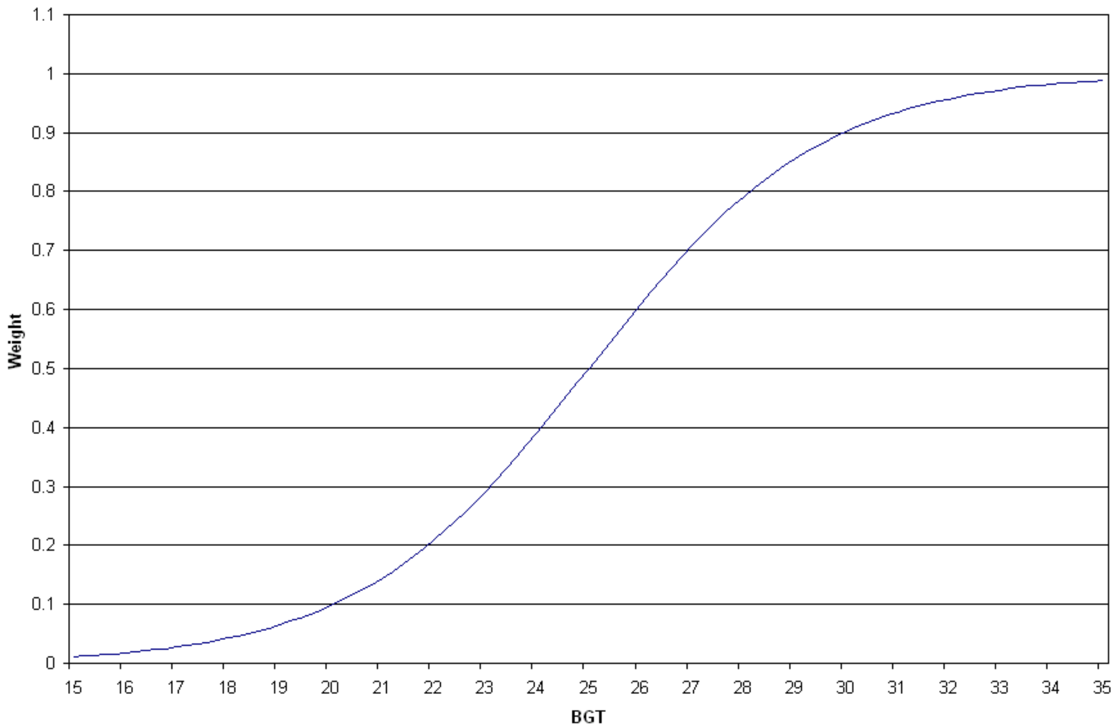

Figure A2: Plot of modified sigmoid function.

Figure A3 shows the forecast HLI values for Amberley plotted against the observed HLI values using the alternative technique described above. Comparing Figure A3 to Figure A1, we see that the outliers have been removed and the gap between the two major clusters is less distinct. This plot is what would be expected for this type of graph. The scatter represents the error inherent in the forecast parameters that were used to calculate the plotted quantities. It should be emphasised that the HLI parameters shown in Figure A1 and Figure A3 are strictly not the same. These have been calculated using different methods and, whilst they are similar, these should not be thought as being the same.

An important issue that must be addressed is how faithfully the HLI values obtained with the new method mimic the HLI values obtained with the current method. There would be little point in developing an alternative method if it did not represent the HLI values as adequately as the existing method. This issue cannot be resolved by relying on the scatter plots alone. Further insight can be gleaned from the temporal behaviour of the relevant variables. This is shown in Figure A4. In this figure, the solid traces represent the HLI time series obtained using the new method with observed and forecast values of relative humidity, temperature and wind speed. The dotted traces represent the HLI time series using the current method with observed and forecast values of relative humidity, temperature and wind speed.

It is evident from Figure A4 that the HLI obtained with the new method compares favourably to the current method. The gross behaviour is reproduced very well – the agreement between the two methods is very good. Discrepancies between the new and current methods exist in the finer detail, however these are of the same magnitude as the discrepancies between forecast and observed values. Overall, it appears that the current method can be upgraded without losing the physical significance of the HLI.

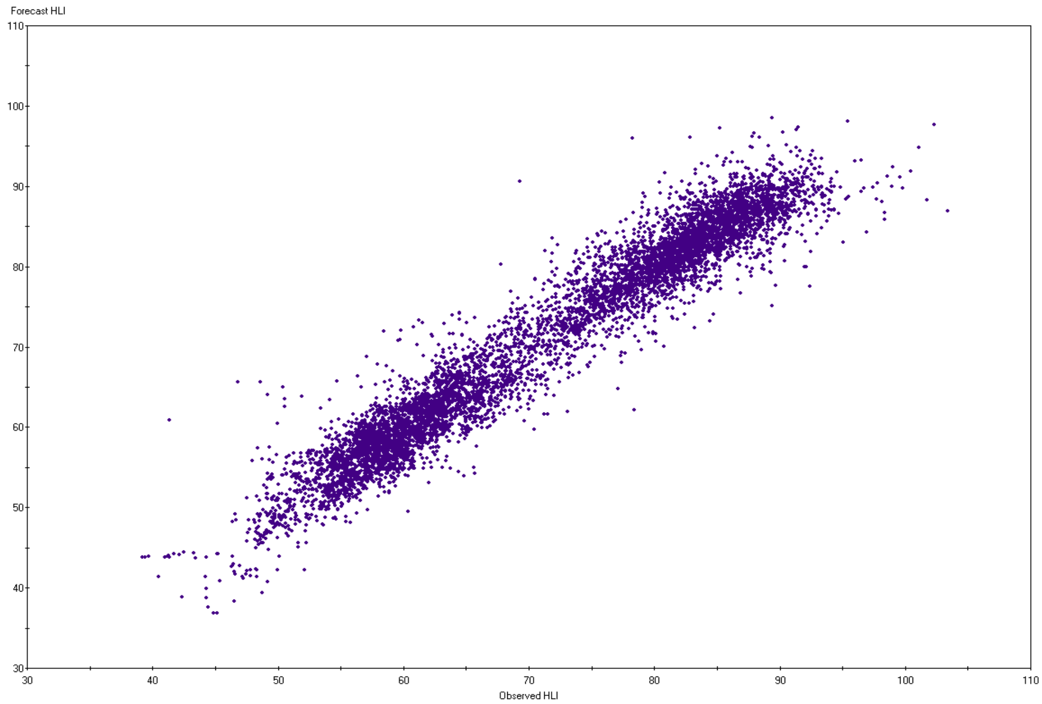

Figure A3: Forecast HLI plotted against Observed HLI. HLI values were calculated using the alternative method.

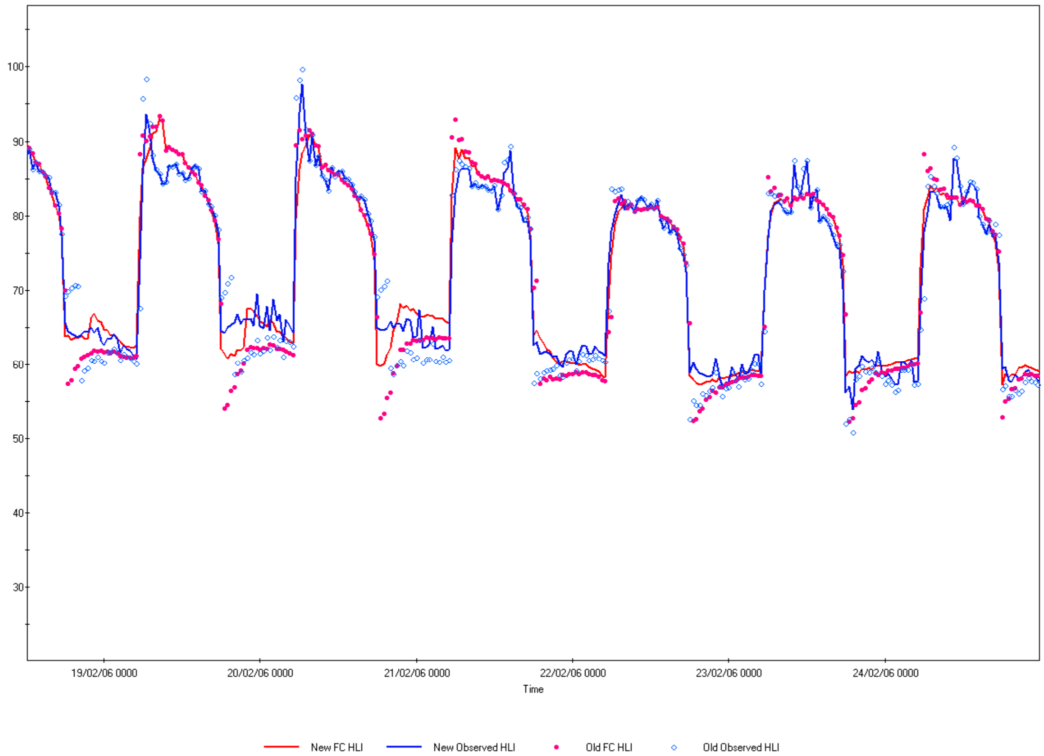

Figure A4: Time series of HLI values calculated using current and alternative methods.

A1.4 Effects of varying the rate parameter “r”

The form of the weighting function is determined by two parameters, “m” and “r”. The “m” parameter shifts the function along the BGT axis thus specifying the BGT value where the contributions from the two expressions for calculating the HLI are equal. The “r” parameter governs the rate that the function switches from one extreme to the other. The size of the BGT interval that the function varies from 0.1 (10%) to 0.9 (90%) is linearly related to “r”. This interval we shall define as the “transition width” or TW. Note that this definition does not result in loss of generality – i.e. choosing values other than 0.1 and 0.9 only changes the proportionality constant relating “r” and the transition width.

To ascertain the effects or varying “r”, HLI values using observed and forecast meteorological parameters were determined and the resulting forecast HLI were plotted against observed HLI for various values of “r”. The results are shown in **Error! Reference source not found.**. The measure used to quantify the effects of various “r” was the Pearson Correlation Coefficient. Also included in the table are the parameters specifying the line of best fit and the transition width associated with each “r” value.

Table A1 Effects of varying “r” on the relationship between forecast and observed HLI values for Amberley

“r”	Transition width, TW	Pearson	Slope	Intercept
0.0	0	0.957	0.961	2.48
0.5	2.2	0.968	0.973	1.62
1.0	4.4	0.970	0.978	1.29
1.5	6.6	0.971	0.979	1.19
2.0	8.8	0.970	0.979	1.21
2.5	11.0	0.969	0.978	1.29
3.0	13.2	0.969	1.01	1.56

From the above table, the following can be deduced:

- The transition width is linearly related to “r”. The relationship is TW = 4.4 * r.
- The original data are well correlated with the outliers forming a small part of the overall population. Consequently, the correlation coefficient is high and any improvements would manifest as small increases in the correlation coefficient.
- The largest increment in the correlation coefficient occurs between “r” = 0 to “r” = 0.5. Thereafter, any increase is relatively small, indicating that even a small amount of “blending” of the two HLI functions produces a noticeable improvement.
- For this data set, the best improvement occurs with an “r” value of 1.5 – i.e. TW of 6.6.
- The weighting function is mathematically undefined for “r” = 0. This case corresponds to an infinitely fast transition between the two expressions used to determine the HLI – it is in fact a mathematical representation of the method currently used.

The above procedure was repeated using data from Charlton, Victoria. The results are shown in Table A2.

Table A2 Effects of varying “r” on the relationship between forecast and observed HLI values for Charlton

“r”	Transition width, TW	Pearson	Slope	Intercept
0.0	0	0.963	0.990	2.67
0.5	2.2	0.968	1.00	2.21
1.0	4.4	0.971	1.00	1.92
1.5	6.6	0.972	1.01	1.76
2.0	8.8	0.973	1.01	1.63
2.5	11.0	0.973	1.01	1.53
3.0	13.2	0.973	1.01	1.45

Comparing **Error! Reference source not found.** to Table A2 shows that the trends are similar in both cases. For Charlton, the effect levels out at a TW of about 8.8. Figure A5 shows the forecast HLI obtained with the current method plotted against the observed HLI. Note again the similarities with the Amberley data. Figure A6 shows the HLIs obtained with the method described here using a TW of 8.8.

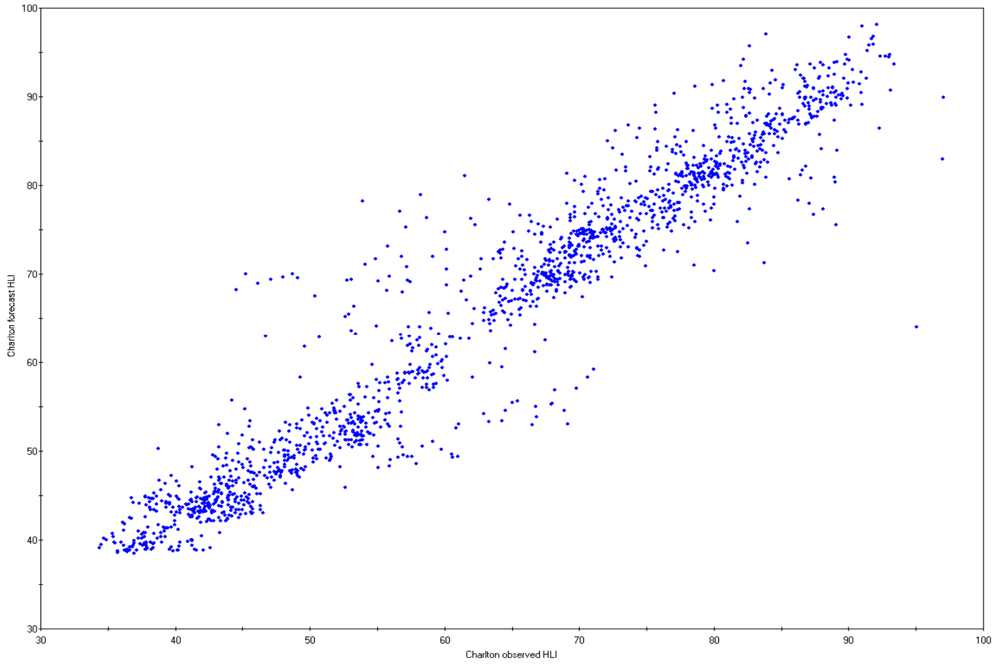

Figure A5 Forecast HLIs plotted against observed HLIs for Charlton using the current method

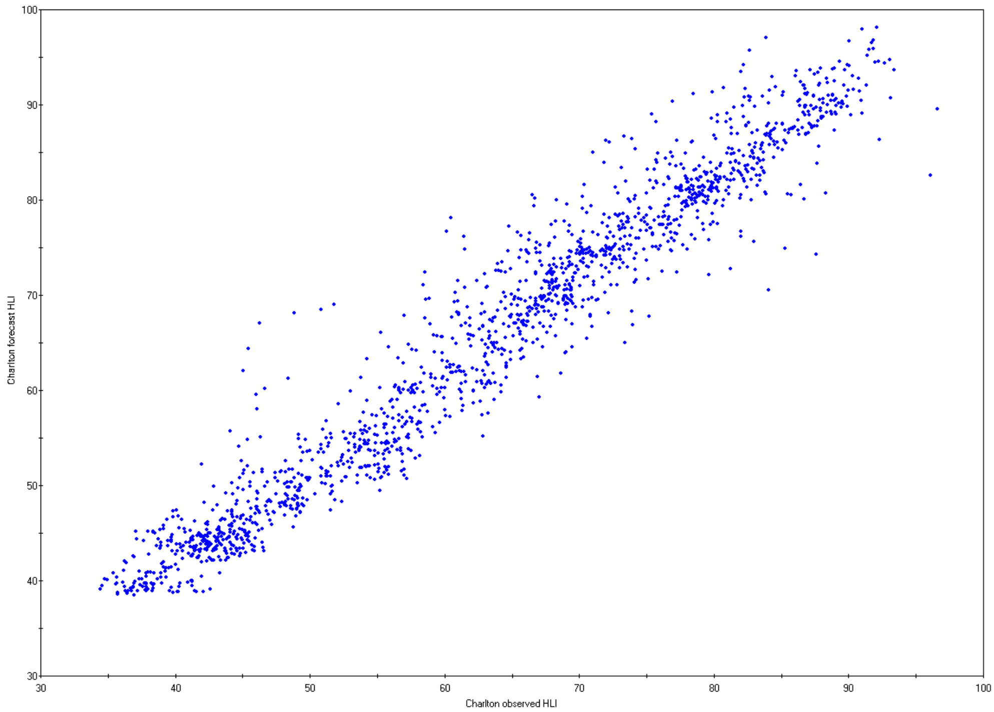

Figure A6 Forecast HLIs plotted against observed HLIs for Charlton using the alternative method

Again the outliers, which initially are small in number, have been removed and the gap between the two major clusters, which is clearly visible in Figure A5 cannot be discerned in Figure A6.

A1.5 AHLU calculations

It has been stated that there are two causes of discrepancies or error between the observed and forecast AHLU. These are the uncertainty inherent in the HLI forecasts and errors introduced by the manner in which the AHLU is calculated. New AHLU values (both forecast and observed) were calculated using the HLI obtained with the method described above. The results – forecast plotted against observed AHLU – showed no noticeable improvement, indicating this error in the HLI is not a major cause of error in the AHLU. Since the number of outliers (the outliers in Figure A1) is small in comparison with the overall data set, we would indeed expect a correspondingly small change in the resultant AHLU. The remaining cause of error - the method used to calculate the AHLU – appears to be the main cause and this will now be discussed.

The calculation of AHLU values shares similarities with HLI calculations in that there are thresholds or sharp cutoffs and different procedures are employed depending on whether the HLI is above or below these thresholds. Complications arise because there are two thresholds: the upper and lower boundaries of the Thermo-Neutral zone. The lower boundary is set at a HLI value of 77. For HLI values below this threshold, the AHLU decreases at a rate of half the difference between the HLI and the threshold. For HLI values above the upper Thermo-Neutral zone threshold, the AHLU increases at a rate equal to the difference between the HLI and the threshold. For HLI values within the Thermo-Neutral zone, the AHLU remains unchanged. Furthermore, the upper Thermo-Neutral zone threshold is variable, depending on the condition of the stock in the feedlot.

Several (but by no means exhaustive) attempts were made at replacing the step functions with continuous functions in a manner similar to that implemented for the HLI calculation, however the results were not satisfactory. Issues which became apparent are:

- The current method calculates an AHLU increment obtained by taking the difference between the HLI value and a threshold. If weighting functions were to be used, an alternative scheme for finding an equivalent to this difference would have to be devised.

- Replacing the two thresholds with two weighting functions is not straight forward as the weighting functions tended to overlap in the Thermo-Neutral zone giving two values for the AHLU increment. It was not clear how a final AHLU increment should be assigned.

- Different weighting functions are required for different upper Thermo-Neutral zone thresholds, although this is a “technical difficulty”, it can be overcome once the other issues are resolved.

The above indicate that a different approach is required to arrive at a method for determining AHLU values that are consistent with the method that is currently used – mainly how the situation for HLI values within the Thermo-Neutral zone should be treated. However, the results obtained for the HLI indicate that avenues based on the approach described above show promise for AHLU calculations and should be investigated further.

A1.6 Summary

An alternative method for calculating the HLI is presented. Investigations into finding an alternative method were carried out because the current method, which utilises two different expressions, can result in large discrepancies in HLI as the transition is made between the two expressions. The HLI values calculated using this alternative method consist of a blend of values from each expression.

Better agreement was found between the HLI values obtained using this method, in that the scatter plot did not show the outliers that result from the sudden switching between the two expressions and that the temporal behaviour of the new HLI values were consistent with values determined using the current method. However, the improved performance of forecasting the HLI did not result in an improvement in the ALHU.

A similar approach was used to implement a method for determining the AHLU, however, this gave unsatisfactory results. It was found that the two thresholds (the upper and lower limits of the Thermo-Neutral zone) and the requirement that the effect on the AHLU be zero for HLI values within the Thermo-Neutral zone ultimately gave rise to poor correlation between the observed and forecast AHLU.

10.2 Appendix B

B1 Terrain analysis

The six MLA feedlots were subjected to a spatial analysis of their terrain and distance to the nearest BoM AWS monitoring site. Figure B1 summarises the results of the spatial analysis.

The complex terrain over the location of the feedlots and the BoM sites show that aside from distance; the differences in the spatial features need to be taken into account to understand the limitations on the suitability of representing meteorology at the sites. Elevation and the orientation of the slope (aspect) are significant drivers in an area's microclimate. To illustrate, a west-facing slope will be warmer than east-facing slopes as the sun's rays are in the west at the hottest time of day. This also impacts on altitudinal and polar limits of tree growth and distribution of vegetation requiring moisture.

While some of the sites show similar aspects, the average distance of the sites from the closest BoM AWS site are 45 km, and the average difference in elevation of 74 m.

As shown in Figure B1 the difference between Oakey (BoM) and Feedlot 1 are apparent based on their location. Feedlot 1 is located closer to the top of the hill on a north-eastern facing slope; while Oakey is located on a north-side facing slope; closer to the bottom of the hill.

The distinction between St. George and Feedlot 2 are apparent, as these two stations are located further apart than any of the other sites.

Tamworth and Feedlot 3, showing a difference of 30 degrees in the aspect, but generally on the same side of a hill, shows a big difference in elevation, due to the distance between the sites.

As shown in Figure B1 and quantified in Table B1 Griffith and Feedlot 4 are located on different sides of a hill.

Deniliquin and Feedlot 5, 60 km apart, show similar aspects and elevation. However, as shown in Figure B1 are located on two different inclines.

Of all the sites, Charlton and Feedlot 6 have the most similar features, located on the same slope, and shown to be the closest sites.

Table B1 Comparison of current forecasting locations (BoM) with feedlot sites (MLA)

Site	Latitude (dd.ddd)	Longitude (ddd.ddd)	Elevation (m)	Aspect (degrees)	Aspect Direction	Distance (km)
Oakey	-27.403	151.741	485.3	9.5	N	18.0
Feedlot 1	-27.524	151.620	555.3	39.9	NE	
St George	-28.049	148.594	297.2	184.8	S	95.0
Feedlot 2	-28.774	149.108	229.5	187.2	S	
Tamworth	-31.074	150.836	644.6	250.3	SW	50.4
Feedlot 3	-31.473	150.584	449.0	284.6	SW	
Griffith	-34.249	146.070	188.5	203.1	SW	33.6
Feedlot 4	-34.114	145.742	132.9	263.7	W	
Deniliquin	-35.558	144.946	94.0	282.2	W	60.2
Feedlot 5	-35.392	144.313	75.8	262.0	W	
Charlton	-36.285	143.334	91.4	332.9	NW	10.8
Feedlot 6	-36.363	143.405	130.1	332.9	NW	

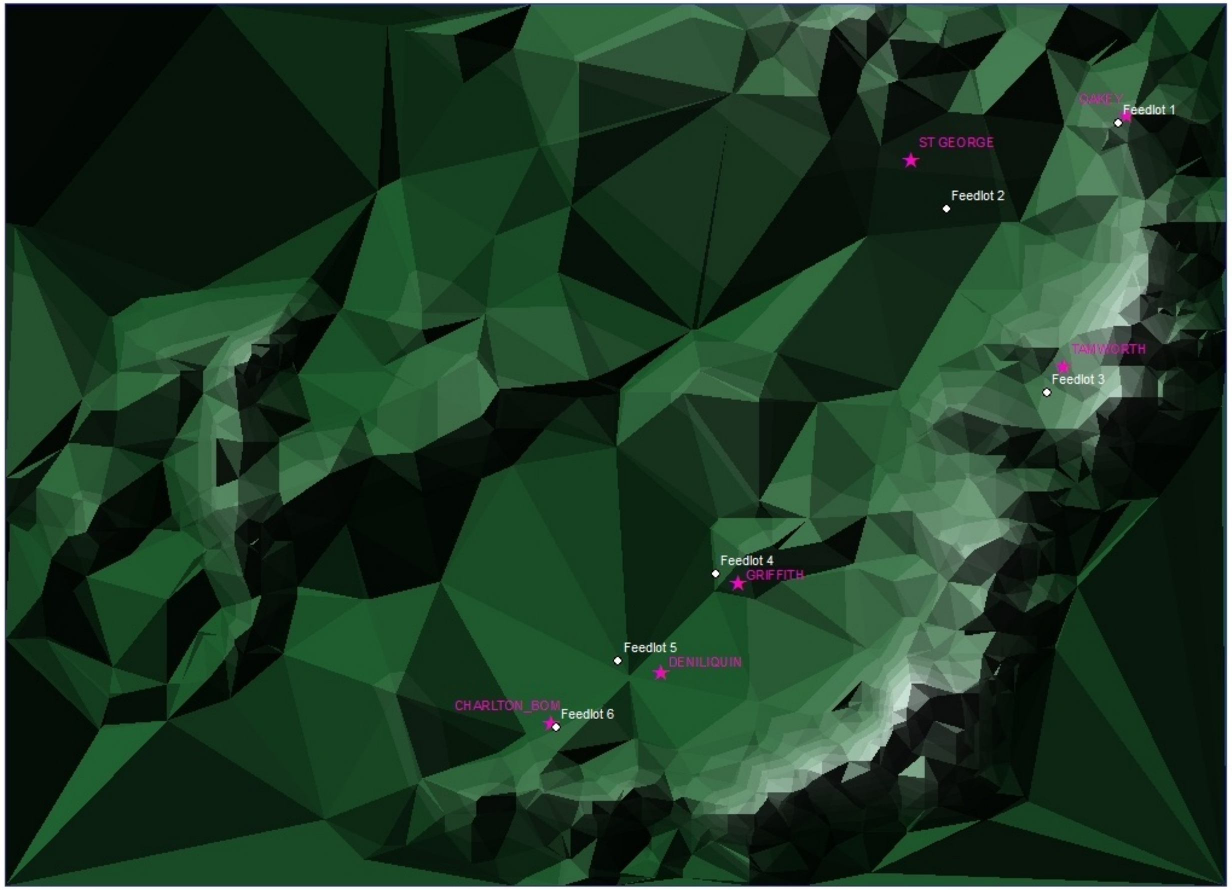

Figure B1 Surface characteristic analysis of BoM AWS sites and MLA registered feedlots

Type:	Data source:	Prepared by:	Date:
Raster/TIN	WRF terrain data	Ella Castillo	July 2010

10.3 Appendix C

C1 Statistical measures

Root Mean Square Error (RMSE)

$$\text{RMSE} = \sqrt{\frac{1}{N}\sum_{i=1}^{N}(P_i - O_i)^2}$$

Equation C1 – Root Mean Square Error

The RSME can be described as the standard deviation of the difference for hourly predicted and observed pairings at a specific point. The RMSE is a quadratic scoring rule which measures the average magnitude of the error. The difference between predicted and corresponding observed values are each squared and then averaged over the sample. Finally, the square root of the average is taken. Since the errors are squared before they are averaged, the RMSE gives a relatively high weight to large errors. This means the RMSE is most useful when large errors are particularly undesirable. Overall, the RSME is a good overall measure of model performance, but since large errors are weighted heavily (due to squaring), its value can be distorted. RMSE is equal to the unit of the values being analysed i.e. an RMSE of 1.2 for wind speed = 1.2 m/s^{-1}.

Systematic Root Mean Square Error (RMSE_s)

$$\text{RMSE}_S = \sqrt{\frac{1}{N}\sum_{i=1}^{N}(\hat{P}_i - O_i)^2}$$

Equation C2 – Systematic Root Mean Square Error

The RMSE_s is calculated as the square root of the mean square difference of hourly predictions from the regression formula and observation pairings, at a specific point. The regressed predictions are taken from the least squares formula. The RMSE_s estimates the model's linear (or systematic) error. The systematic error is a measure of the bias in the model due to user input or model deficiency, i.e. data input errors, assimilation variables, choice of model options etc.

Unsystematic Root Mean Square Error (RMSE_u)

$$\text{RMSE}_U = \sqrt{\frac{1}{N}\sum_{i=1}^{N}(\hat{P}_i - P_i)^2}$$

Equation C3 – Unsystematic Root Mean Square Error

The RMSE_u is calculated as the square root of the mean square difference of hourly predictions from the regression formula and model prediction value pairings, at a specific point. The RMSE_u is a measure of how much of the difference between predictions and observations resulting from random processes or influences outside the legitimate range of the model. This error may require model refinement, such as new algorithms or higher resolution grids, or that the phenomena being simulated cannot be fully resolved by the model.

Ultimately for 'good' model performance, the RMSE should be a low value, with most of the variation explained in the observations. Here, the systematic error $RMSE_s$ should approach zero and the unsystematic error, $RMSE_u$, should approach the RMSE since:

$$\mathrm{RMSE}^2 = \mathrm{RMSE}_\mathrm{S}^2 + \mathrm{RMSE}_\mathrm{u}^2$$

Equation C4

Mean Error (ME) and Mean Absolute Error (MAE)

The ME is simply the average of the hourly modelled values minus the hourly observed values. It contains both systematic and unsystematic errors and is heavily influence by high and low errors.)

The MAE measures the average magnitude of the errors in a set of predictions, without considering their direction. It measures accuracy for continuous variables. Expressed in words, the MAE is the average over the verification sample of the absolute values of the differences between predictions and the corresponding observation. The MAE is a linear score which means that all the individual differences are weighted equally in the average. The MAE and the RMSE can be used together to diagnose the variation in the errors in a set of predictions. The RMSE will always be larger or equal to the MAE; the greater difference between them, the greater the variance in the individual errors in the sample. If the RMSE=MAE, then all the errors are of the same magnitude Both the MAE and RMSE can range from 0 to ∞. They are negatively-oriented scores: Lower values are better.

Skill measure statistics are given in terms of a score, rather than in absolute terms.

Index of agreement

$$\mathrm{IOA} = 1 - \frac{\sum_{i=1}^{N} (P_i - O_i)^2}{\sum_{i=1}^{N} (|P_i - O_{mean}| + |O_i - O_{mean}|)^2}$$

Equation C5 – Index of Agreement

The IOA is calculated using a method described in Willmott (1982). The IOA can take a value between 0 and 1, with 1 indicating perfect agreement. The IOA is the ratio of the total RMSE to the sum of two differences: the difference between each prediction and the observed mean, and the difference between each observation and observed mean. From another perspective, the IOA is a measure of the match between the departure of each prediction from the observed mean and the departure of each observation from the observed mean

(Note: N is the number of observations, Pi are the hourly model predictions, Oi are the hourly observations, O_{mean} is the observed observation mean, and $\hat{P}_i = a + bO_i$ is the linear regression fitted with intercepts a and slope *b*.)

Pearson Correlation Coefficient

The Pearson Correlation Coefficient is a measure of the strength of the linear relationship between the predicted and observed measurements (defined in Equation C6). The closer this value is to unity the stronger the relationship.

$$r = \frac{N\left(\sum_{i=1}^{N} O_i\, P_i\right) - \left(\sum_{i=1}^{N} O_i\right)\left(\sum_{i=1}^{N} P_i\right)}{\sqrt{\left[N\left(\sum_{i=1}^{N} O_i^2\right) - \left(\sum_{i=1}^{N} O_i\right)^2\right]\left[N\left(\sum_{i=1}^{N} P_i^2\right) - \left(\sum_{i=1}^{N} P_i\right)^2\right]}}$$

Equation C6 – Pearson Correlation Coefficient

10.4 Appendix D

D1 Sensitivity analysis

The HLI value at any hour depends, to varying degrees, on the following variables: Temperature (T), Relative Humidity (RH), Wind Speed (WS) and Solar Radiation (SR). In practice, the Solar Radiation and Temperature are combined into a single variable, the Black Globe Temperature (BGT). The degree to which the HLI depends on each variable, combined with the accuracy of the forecast for the variable, determines the accuracy of the HLI forecast. For example, if the HLI is not sensitive to SR, meaning that a large change in SR results in minimal change in HLI, then poor forecasts of SR will not result in significantly poor HLI forecasts.

When analysing the sensitivity of the response, or output, of a system to changes in input parameters, the sensitivity is usually stated in terms of fractional or percentage changes – changing the input by a certain percentage causes the output to change by some (different) percentage. If a specified percentage change in the input causes the same percentage change in the output then the system is a linear system. In practice most real systems are not linear; therefore the sensitivity depends on the state of the system.

In applying sensitivity analyses to the HLI, the “system” is the equation (or equations) used to calculate the HLI, the input parameters are T, WS, SR, RH and the output is the HLI value. The dependence of the HLI on RH is linear, however, the dependence on T is a mixture of linear and a square root function, the dependence on WS is a combination of linear and exponential and the dependence of SR is logarithmic. The analysis is further complicated because there are two separate equations that are used to calculate the HLI, depending on whether the BGT is greater than 25.

However, we note that for high heat stress situations, the HLI is calculated using predominantly one equation – the equation used for a BGT greater than 25 degrees:

$$HLI_{HI} = 1.55*BGT + 0.38*RelHum - 0.5*WSpeed + \exp(2.4 - WSpeed) + 8.62$$

where

$$BGT = 1.33*Temp - 2.65*\sqrt{Temp} + 3.21*\log(SolRad + 1) + 3.5$$

where
sqrt(…) is the square root function,
log(…) is the logarithmic function and
exp(…) is the exponential function.

As this represents the important scenario, a sensitivity analysis will be performed on this equation.

D2 Relative Humidity

Inspection of the above equations shows that the only term involving RH includes a multiplicative constant of 0.38. Thus, to obtain the change in HLI given that only RH changes, the change in HLI is the change in RH multiplied by 0.38. For example, if RH increases from 60% to 70%, ie a change of 10%, then the HLI increases by 10 x 0.38 = 3.8.

D3 Temperature

Table D1 shows the change in HLI that result from a change in temperature for various temperatures. For example, at a temperature of 25 ºC, a 1 ºC temperature rise would result in a HLI increase of about 1.65.

Table D1 Temperature sensitivity analysis

Temperature (°C)	Change in HLI for 1ºC change
20	1.60
25	1.65
30	1.68
35	1.71
40	1.73

D4 Wind Speed

Table D2 shows the change in HLI that results from a change in wind speed for various wind speeds. For example, at a wind speed of 6 m/s, a 1 m/s increase would result in a HLI decrease of approximately 0.5 units.

Table D2 Wind speed sensitivity analysis

Wind Speed (m/s)	Change in HLI for 1m/s change
2	-1.99
4	-0.70
6	-0.50
8	-0.50
10	-0.50

D5 Solar radiation

Table D3 shows the change in HLI that results from a change in solar radiation for various values of solar radiation. For example, at a level of 600 W/m^2, a 100 W/m^2 increase would result in a HLI increase of about 0.4.

Table D3 Solar radiation sensitivity analysis

Solar Radiation (W/m^2)	Change in HLI for 100 W/m^2 change
200	1.1
400	0.5
600	0.4
800	0.3
1000	0.2

In assessing the impact on the HLI due to poor forecasts of the input variables, the absolute values of the input parameters should be taken into consideration. For example, relative humidity can vary from about 0% to 100%. An error of one tenth of this range (10%) gives rise to an error in the HLI of 3.8. The temperature could range from 0 ºC to 40 ºC. An error in the temperature forecast of one tenth of this range (4 ºC) gives rise to an error between 6.4 and 6.8 in HLI, depending on the actual temperature – about twice the error compared to the corresponding case for the relative humidity. A similar situation exists for the wind speed. The HLI is relatively insensitive to changes in solar radiation except at very low solar radiation levels such as on very overcast days.

Appendix E

E1 Heat load index

Table E1 Performance statistics of the upgraded system prediction of heat load index

Parameter	intercept	slope	r^2	RMSE	$RMSE_s$	$RMSE_u$	IOA	RCOR	ME	MAE
Emerald	12.25	0.82	0.84	5.56	2.94	4.72	0.95	0.92	-1.70	4.17
Mareeba	5.93	0.88	0.78	7.23	3.72	6.19	0.93	0.88	-3.34	5.18
Oakey	2.51	0.92	0.85	5.66	3.08	4.75	0.95	0.92	-2.91	3.79
Deniliquin	4.53	0.93	0.82	5.95	0.97	5.87	0.95	0.90	-0.05	4.30
Griffith	7.34	0.86	0.78	6.86	2.83	6.25	0.93	0.88	-2.12	4.81
St George	-4.15	1.00	0.76	7.88	4.31	6.59	0.90	0.87	-4.31	5.69
Tamworth	0.70	0.90	0.88	7.75	6.10	4.78	0.93	0.94	-5.94	6.40
Charlton	3.39	0.92	0.74	7.26	2.31	6.88	0.92	0.86	-2.05	4.96
Katanning	10.77	0.83	0.67	6.85	2.00	6.55	0.90	0.82	0.32	4.07
Southern Cross	5.76	0.90	0.71	7.05	1.54	6.88	0.92	0.85	-0.87	4.36
Morawa	5.07	0.90	0.67	8.00	1.91	7.77	0.90	0.82	-1.44	5.21
Minipa	6.19	0.92	0.85	4.84	1.64	4.55	0.96	0.92	1.36	2.82
Port Augusta	9.30	0.85	0.84	5.21	2.01	4.80	0.95	0.91	-0.44	3.38
Warra	9.59	0.83	0.81	4.23	1.65	3.90	0.95	0.90	-0.15	2.41

Table E2 Performance statistics of the current system prediction of heat load index

Parameter	intercept	slope	r^2	RMSE	$RMSE_s$	$RMSE_u$	IOA	RCOR	ME	MAE
Emerald	5.44	0.89	0.90	5.34	3.67	3.87	0.96	0.95	-3.35	4.23
Mareeba	1.57	0.98	0.92	3.77	0.30	3.76	0.98	0.96	0.16	2.72
Oakey	3.10	0.93	0.93	3.74	2.03	3.14	0.98	0.96	-1.82	2.85
Deniliquin	0.29	1.01	0.91	4.43	1.23	4.26	0.97	0.95	1.22	3.17
Griffith	-3.43	1.01	0.88	5.84	2.69	5.18	0.96	0.94	-2.69	4.46
St George	-0.60	1.00	0.85	4.86	0.59	4.82	0.96	0.92	-0.59	3.42
Tamworth	6.96	0.91	0.93	3.93	1.42	3.67	0.98	0.96	0.55	3.04
Charlton	1.13	0.98	0.90	4.41	0.48	4.38	0.97	0.95	-0.37	2.88
Katanning	8.43	0.83	0.88	4.27	2.42	3.52	0.96	0.94	-1.52	2.48
Southern Cross	2.36	0.97	0.93	3.42	0.80	3.33	0.98	0.96	0.74	2.09
Morawa	0.82	0.99	0.95	2.78	0.23	2.77	0.99	0.98	0.19	1.65
Minipa	3.02	0.94	0.90	3.76	0.84	3.66	0.97	0.95	-0.50	2.04
Port Augusta	1.06	1.00	0.90	4.52	1.06	4.40	0.97	0.95	1.06	2.50
Warra	6.30	0.89	0.84	4.01	1.10	3.86	0.95	0.91	-0.14	2.24

E2 Temperature

Table E3 Performance statistics of the upgraded system prediction of temperature

Parameter	intercept	slope	r^2	RMSE	$RMSE_s$	$RMSE_u$	IOA	RCOR	ME	MAE
Emerald	2.70	0.92	0.82	1.47	0.59	1.34	0.95	0.91	0.53	1.07
Mareeba	3.21	0.86	0.83	1.39	0.56	1.27	0.95	0.91	-0.31	1.04
Oakey	3.36	0.79	0.84	2.28	1.83	1.36	0.91	0.92	-1.61	1.89
Deniliquin	5.52	0.79	0.73	2.97	1.38	2.63	0.92	0.85	0.76	2.25
Griffith	6.45	0.75	0.72	2.56	1.27	2.22	0.91	0.85	0.46	1.89
St George	3.52	0.89	0.81	1.84	0.91	1.60	0.94	0.90	0.81	1.36
Tamworth	5.04	0.74	0.83	2.40	1.72	1.68	0.93	0.91	-1.10	1.82
Charlton	5.08	0.77	0.82	2.57	1.37	2.17	0.94	0.90	0.03	2.02
Katanning	2.18	0.86	0.90	2.25	1.24	1.88	0.97	0.95	-0.81	1.52
Southern Cross	0.14	0.95	0.89	2.69	1.20	2.41	0.96	0.94	-1.14	2.19
Morawa	-0.73	0.97	0.93	2.36	1.62	1.71	0.97	0.97	-1.61	2.00
Minipa	2.91	0.93	0.91	2.30	1.43	1.81	0.97	0.96	1.35	1.73
Port Augusta	2.27	0.88	0.90	2.14	1.11	1.84	0.97	0.95	-0.80	1.72
Warra	1.36	0.90	0.83	1.90	0.51	1.83	0.95	0.91	-0.21	1.49

Table E4 Performance statistics of the current system prediction of temperature

Parameter	intercept	slope	r^2	RMSE	$RMSE_s$	$RMSE_u$	IOA	RCOR	ME	MAE
Emerald	5.33	0.81	0.84	1.30	0.65	1.13	0.95	0.91	0.23	0.97
Mareeba	3.65	0.87	0.86	1.31	0.59	1.17	0.96	0.93	0.41	0.83
Oakey	5.53	0.75	0.83	1.75	1.09	1.38	0.94	0.91	-0.37	1.46
Deniliquin	1.29	0.93	0.86	2.12	0.54	2.05	0.96	0.93	-0.36	1.63
Griffith	2.17	0.92	0.77	2.58	0.52	2.52	0.93	0.88	0.34	1.93
St George	4.08	0.81	0.67	2.28	0.91	2.09	0.90	0.82	-0.59	1.61
Tamworth	1.96	0.90	0.89	1.70	0.71	1.55	0.97	0.94	-0.49	1.36
Charlton	0.97	0.97	0.90	2.01	0.36	1.98	0.97	0.95	0.31	1.53
Katanning	3.14	0.81	0.82	2.89	1.45	2.50	0.94	0.90	-0.77	2.08
Southern Cross	2.75	0.91	0.92	2.10	0.78	1.95	0.98	0.96	0.40	1.45
Morawa	1.17	0.97	0.96	1.35	0.37	1.30	0.99	0.98	0.30	1.06
Minipa	2.01	0.88	0.93	1.79	0.93	1.53	0.98	0.96	-0.54	1.32
Port Augusta	2.45	0.90	0.93	1.64	0.61	1.52	0.98	0.96	0.01	1.28
Warra	2.77	0.82	0.79	2.06	0.80	1.90	0.94	0.89	0.05	1.59

E3 Relative humidity

Table E5 Performance statistics of the upgraded system prediction of relative humidity

Parameter	intercept	slope	r^2	RMSE	$RMSE_s$	$RMSE_u$	IOA	RCOR	ME	MAE
Emerald	7.51	0.75	0.73	15.36	13.03	8.15	0.82	0.86	-12.26	12.75
Mareeba	12.51	0.76	0.56	14.25	8.35	11.55	0.83	0.75	-7.23	10.67
Oakey	18.75	0.8	0.79	9.57	5.46	7.86	0.93	0.89	3.9	7.52
Deniliquin	27.58	0.47	0.46	19.1	14.45	12.5	0.78	0.68	-6.52	14.17
Griffith	25.29	0.49	0.41	20.15	14.76	13.72	0.76	0.64	-8.46	15.96
St George	7.8	0.71	0.47	19.52	14.23	13.36	0.75	0.68	-13.25	14.53
Tamworth	23.84	0.54	0.48	15.34	11.42	10.24	0.79	0.69	-7.85	11.86
Charlton	25.16	0.58	0.64	15.7	11.2	11.01	0.87	0.8	-3.23	12.21
Katanning	8.99	1.01	0.82	13.6	9.62	9.62	0.9	0.91	9.62	11.37
Southern Cross	10.4	0.85	0.67	14.11	4.87	13.25	0.9	0.82	3.48	10.25
Morawa	4.51	0.96	0.81	10.71	3.22	10.21	0.94	0.9	3.13	7.78
Minipa	2.23	0.88	0.84	10.94	5.84	9.25	0.94	0.92	-5.09	8.01
Port Augusta	11.44	0.8	0.6	13.08	3.97	12.46	0.88	0.77	1.45	9.86
Warra	28.46	0.67	0.54	11.96	6.04	10.32	0.85	0.74	2.34	8.78

Table E6 Performance statistics of the upgraded system prediction of relative humidity

Parameter	intercept	slope	r^2	RMSE	$RMSE_s$	$RMSE_u$	IOA	RCOR	ME	MAE
Emerald	12.26	0.78	0.75	10.62	7.05	7.94	0.9	0.87	-5.79	7.47
Mareeba	8.3	0.85	0.8	8.63	4.62	7.29	0.93	0.89	-3.85	5.98
Oakey	20.04	0.79	0.83	9.09	6	6.83	0.93	0.91	4.48	7.52
Deniliquin	16.91	0.76	0.75	12.39	6	10.84	0.92	0.86	1.65	9.17
Griffith	21.71	0.64	0.63	14.09	8.6	11.15	0.88	0.79	-2.22	10.02
St George	21.22	0.68	0.5	13.45	5.8	12.14	0.84	0.71	-1.55	9.4
Tamworth	11.57	0.89	0.77	9.57	4.36	8.52	0.92	0.88	3.93	6.96
Charlton	14.49	0.79	0.8	11.36	5.41	9.99	0.94	0.9	0.41	8.63
Katanning	9.63	0.87	0.79	9.65	3.34	9.05	0.94	0.89	2.07	7.58
Southern Cross	2.88	0.92	0.81	10.04	2.15	9.8	0.95	0.9	-0.99	6.55
Morawa	1.41	0.94	0.93	6.03	1.77	5.77	0.98	0.96	-1.09	4.27
Minipa	17.16	0.7	0.86	9.99	7.38	6.74	0.94	0.93	-1.42	8.08
Port Augusta	14.88	0.73	0.64	11.62	5.19	10.4	0.89	0.8	1.3	8.66
Warra	24.34	0.69	0.57	11.26	5.32	9.93	0.87	0.76	-0.49	8.77

E4 Wind speed

Table E7 Performance statistics of the upgraded system prediction of wind speed

Parameter	intercept	slope	r^2	RMSE	$RMSE_s$	$RMSE_u$	IOA	RCOR	ME	MAE
Emerald	1.88	0.55	0.25	1.50	0.76	1.29	0.69	0.50	0.46	1.20
Mareeba	2.95	0.40	0.15	2.51	1.89	1.65	0.57	0.38	1.60	2.01
Oakey	2.22	0.61	0.45	2.14	1.06	1.85	0.82	0.67	0.02	1.64
Deniliquin	1.64	0.47	0.27	2.08	1.39	1.54	0.70	0.52	-0.89	1.62
Griffith	1.94	0.41	0.22	2.08	1.34	1.59	0.68	0.47	-0.54	1.59
St George	2.40	0.65	0.31	2.27	1.28	1.88	0.70	0.56	1.08	1.77
Tamworth	2.41	0.44	0.34	2.21	1.58	1.55	0.74	0.59	0.74	1.80
Charlton	1.91	0.54	0.25	1.85	0.84	1.65	0.71	0.50	0.27	1.43
Katanning	2.89	0.28	0.20	2.36	1.94	1.35	0.58	0.44	-0.84	1.36
Southern Cross	2.55	0.44	0.25	1.99	1.22	1.57	0.70	0.50	-0.30	1.56
Morawa	1.09	0.75	0.45	1.53	0.47	1.45	0.81	0.67	-0.20	1.16
Minipa	1.67	0.50	0.40	1.80	1.32	1.22	0.74	0.63	-0.88	1.38
Port Augusta	1.74	0.48	0.34	2.31	1.71	1.56	0.70	0.58	-1.20	1.85
Warra	1.67	0.55	0.32	1.59	0.94	1.28	0.72	0.57	0.62	1.22

Table E8 Performance statistics of the upgraded system prediction of wind speed

Parameter	intercept	slope	r^2	RMSE	$RMSE_s$	$RMSE_u$	IOA	RCOR	ME	MAE
Emerald	3.30	0.73	0.23	3.06	2.48	1.79	0.49	0.48	2.45	2.56
Mareeba	1.14	0.29	0.15	1.74	1.28	1.17	0.63	0.39	-0.46	1.40
Oakey	-0.30	1.75	0.60	5.92	4.46	3.90	0.61	0.78	3.96	4.23
Deniliquin	1.26	0.48	0.29	2.20	1.62	1.48	0.68	0.54	-1.23	1.66
Griffith	4.34	0.75	0.30	4.04	3.31	2.32	0.52	0.55	3.27	3.47
St George	1.27	0.37	0.19	2.21	1.65	1.47	0.63	0.44	-1.10	1.72
Tamworth	0.98	0.57	0.51	1.86	1.16	1.45	0.82	0.71	-0.32	1.32
Charlton	3.52	0.67	0.20	3.33	2.39	2.33	0.52	0.45	2.32	2.88
Katanning	5.06	0.32	0.17	2.82	2.26	1.68	0.56	0.42	1.56	1.94
Southern Cross	1.97	0.49	0.36	1.84	1.21	1.38	0.75	0.60	-0.59	1.40
Morawa	0.75	0.82	0.55	1.34	0.38	1.29	0.85	0.74	-0.20	1.03
Minipa	1.84	0.63	0.44	1.58	0.74	1.40	0.81	0.66	-0.08	1.25
Port Augusta	3.18	0.35	0.15	2.51	1.58	1.94	0.64	0.39	-0.46	1.83
Warra	1.08	0.33	0.20	1.58	1.18	1.05	0.64	0.45	-0.50	1.29

10.5 Appendix F

FEEDLOT 1 STATISTICS AND FIGURES

Table F1 Summary statistics of meteorology and heat load index measured onsite and modelled in WRF and KAT for Feedlot 1

Parameter	Average	Standard Deviation	Minimum	Maximum
MLA HLI	65.45	12.24	42.67	91.07
WRF HLI	66.06	12.74	45.63	90.49
KAT HLI	65.70	11.92	45.65	87.11
MLA Temperature (°C)	23.12	4.24	17.80	35.10
WRF Temperature (°C)	21.97	3.46	16.31	31.17
KAT Temperature (°C)	22.85	3.31	17.11	32.02
MLA Relative Humidity (%)	72.13	22.64	22.00	104.00
WRF Relative Humidity (%)	77.78	17.34	26.29	97.77
KAT Relative Humidity (%)	78.78	16.58	36.67	100.00
MLA Wind speed (m/s)	7.14	3.69	0.65	16.85
WRF Wind speed (m/s)	5.84	2.62	0.16	12.56
KAT Wind speed (m/s)	9.65	6.18	1.20	31.69

Table F2 Performance statistics of meteorology and heat load index measured onsite and modelled in WRF and KAT for Feedlot 1

Parameter	Intercept	Slope	r^2	RMSE	$RMSE_s$	$RMSE_u$	IOA	RCOR	ME
WRF HLI	0.19	1.01	0.93	3.31	0.62	3.25	0.98	0.97	0.62
KAT HLI	4.52	0.93	0.92	3.46	0.84	3.35	0.98	0.96	0.25
WRF Temperature (°C)	4.56	0.75	0.86	2.03	1.55	1.31	0.93	0.93	-1.15
KAT Temperature (°C)	6.49	0.71	0.82	1.88	1.27	1.38	0.94	0.91	-0.27
WRF Relative Humidity (%)	28.77	0.68	0.79	12.17	9.19	7.98	0.91	0.89	5.65
KAT Relative Humidity (%)	31.80	0.65	0.79	12.79	10.32	7.56	0.89	0.89	6.65
WRF Wind speed (m/s)	2.50	0.47	0.43	3.07	2.35	1.97	0.76	0.66	-1.30
KAT Wind speed (m/s)	0.15	1.33	0.63	4.67	2.79	3.74	0.77	0.80	2.51

a) February Forecast

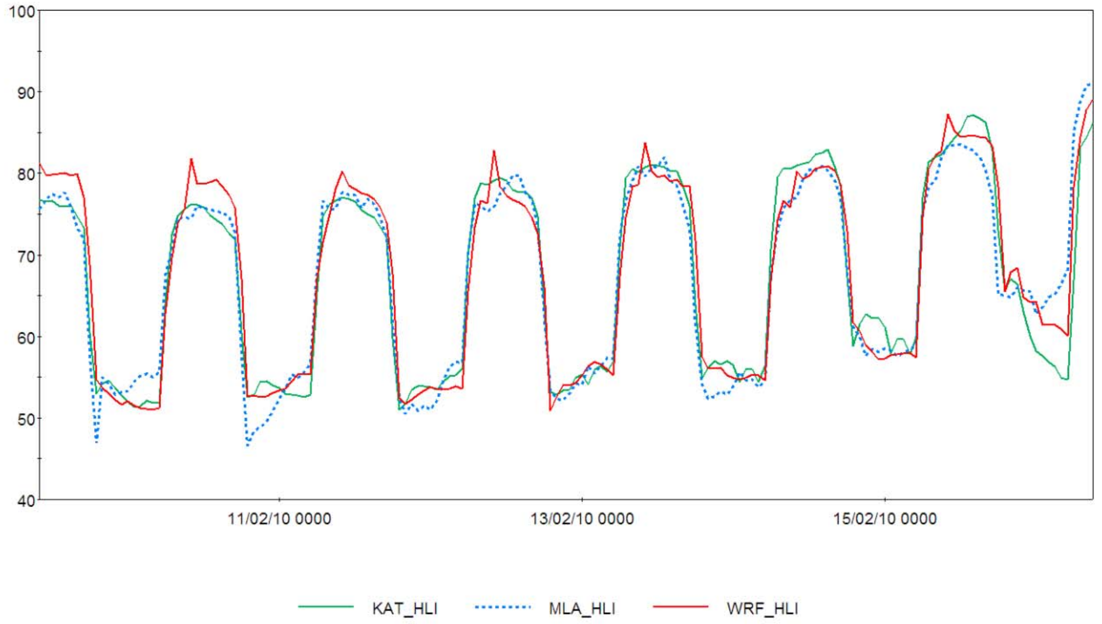

b) March Forecast

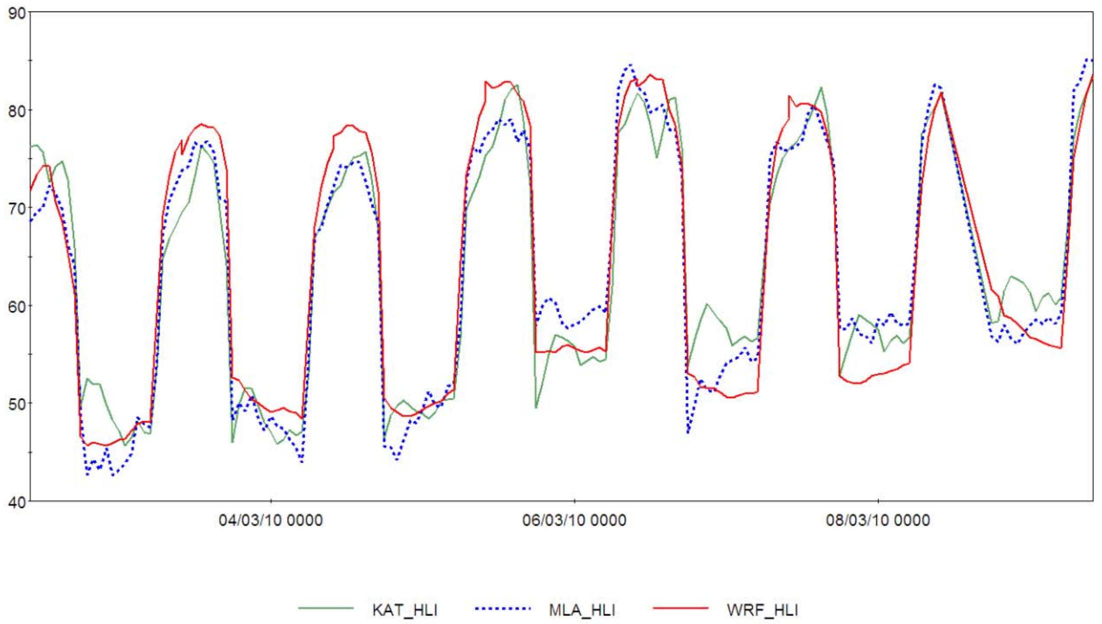

Figure F1 Heat Load Index (HLI) at Feedlot 1 calculated by MLA, KAT and WRF for the forecast assessment periods

Location: Feedlot 1	Period: February and March 2010	Data source: MLA,KAT and WRF	Units: HLI
Type: Time series		Prepared by: Andrew Vernon	Date: July 2010

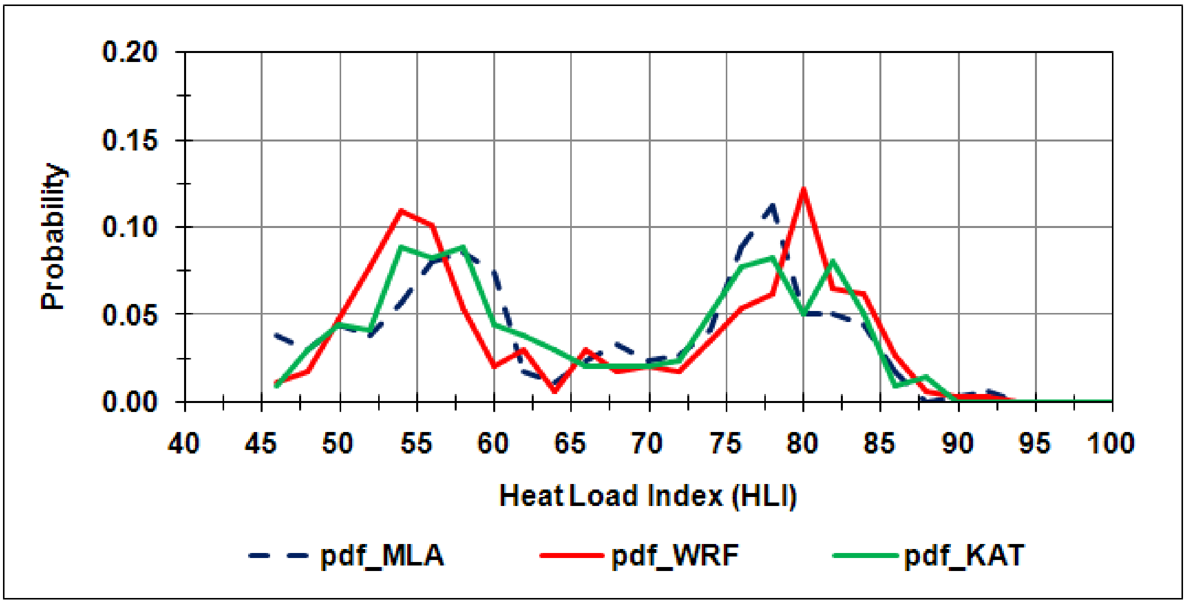

Figure F2	Heat Load Index (HLI) probability density function (pdf) at Feedlot 1 for MLA, KAT and WRF		
Location: Feedlot 1	Period: February and March 2010	Data source: MLA,KAT and WRF	Units: probability
Type: pdf plot		Prepared by: Andrew Vernon	Date: July 2010

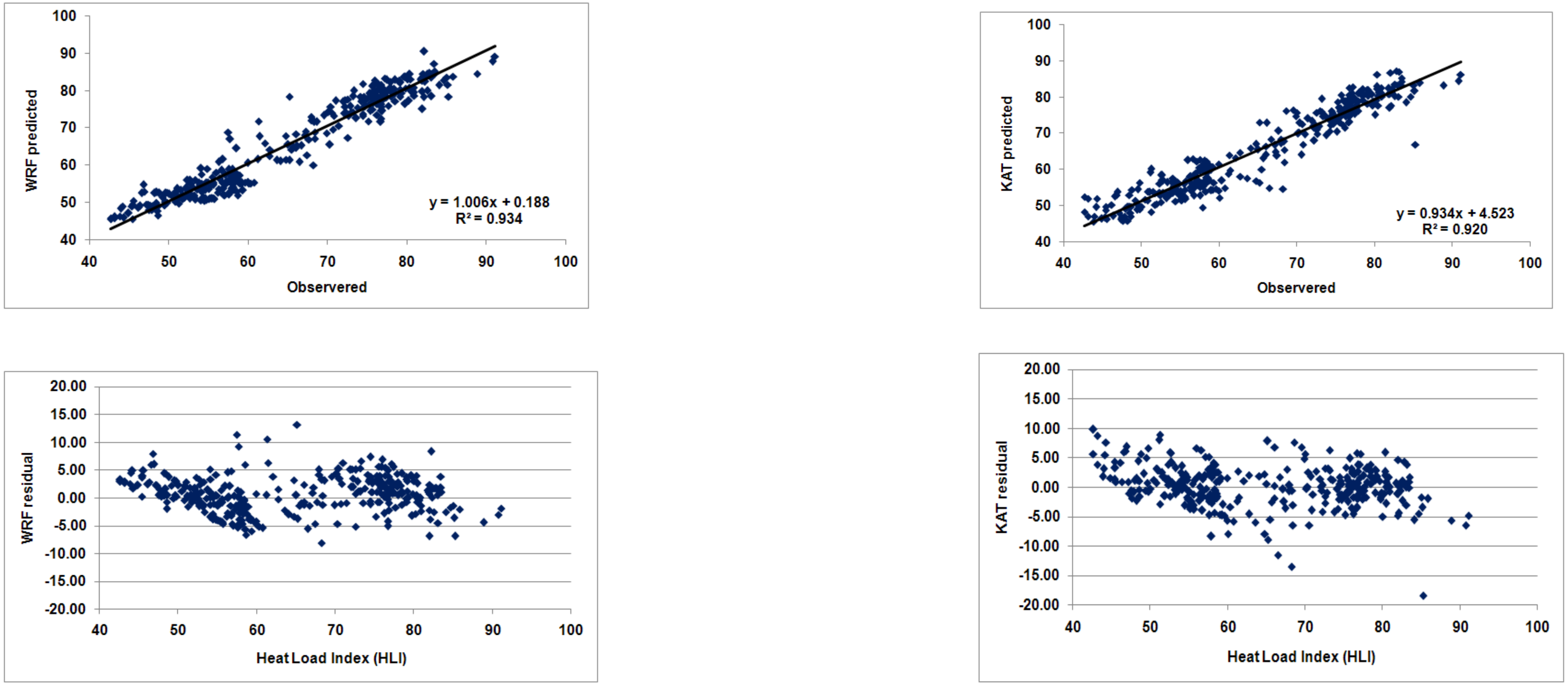

Figure F3 Regression and residual plots of HLI from KAT and WRF predictions at Feedlot 1

Type:	Data source:	Prepared by:	Date:
Regression and residuals charts	KAT and WRF	Andrew Vernon	July 2010

FEEDLOT 2 STATISTICS AND FIGURES

Table F3 Summary statistics of meotorology and heat load index measured onsite and modelled in WRF and KAT for Feedlot 2

Parameter	Average	Standard Deviation	Minimum	Maximum
MLA_HLI	72.54	12.09	53.16	93.35
WRF_HLI	68.93	13.58	43.05	95.78
KAT_HLI	71.17	12.58	41.72	96.85
MLA HLI	25.42	4.34	15.85	35.80
WRF HLI	25.80	3.69	16.02	34.23
KAT HLI	24.51	3.47	17.65	36.58
MLA Temperature (°C)	65.73	19.76	27.00	96.00
WRF Temperature (°C)	57.36	17.60	23.04	94.03
KAT Temperature (°C)	68.39	15.42	23.40	100.00
MLA Relative Humidity (%)	2.17	1.22	0.00	5.74
WRF Relative Humidity (%)	4.36	1.99	0.11	9.42
KAT Relative Humidity (%)	2.41	1.35	0.35	10.18

Table F4 Performance statistics of meotorology and heat load index measured onsite and modelled in WRF and KAT for Feedlot 2

Parameter	Intercept	Slope	r^2	RMSE	$RMSE_s$	$RMSE_u$	IOA	RCOR	ME
WRF HLI	-8.22	1.06	0.90	5.70	3.69	4.34	0.95	0.95	-3.61
KAT HLI	-0.04	0.98	0.89	4.37	1.39	4.15	0.97	0.94	-1.37
WRF Temperature (°C)	6.72	0.75	0.78	2.07	1.15	1.72	0.93	0.88	0.38
KAT Temperature (°C)	8.19	0.64	0.64	2.74	1.80	2.07	0.87	0.80	-0.91
WRF Relative Humidity (%)	14.45	0.65	0.54	16.12	10.81	11.95	0.82	0.73	-8.37
KAT Relative Humidity (%)	35.64	0.50	0.41	15.67	10.25	11.85	0.78	0.64	2.66
WRF Wind speed (m/s)	2.59	0.82	0.25	2.79	2.20	1.72	0.49	0.50	2.19
KAT Wind speed (m/s)	1.86	0.25	0.05	1.62	0.94	1.32	0.54	0.23	0.24

a) February Forecast

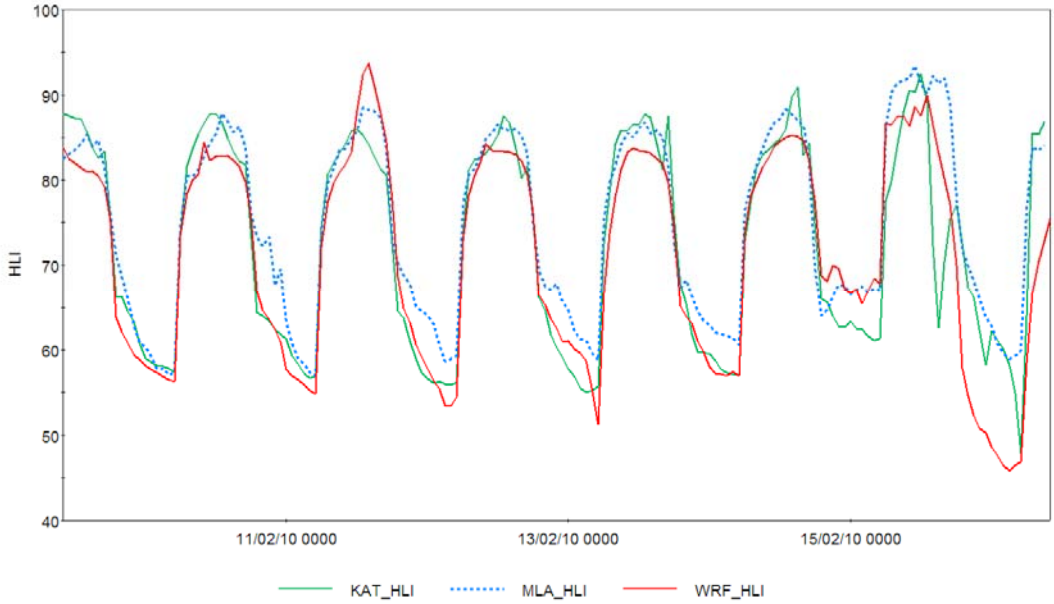

b) March Forecast

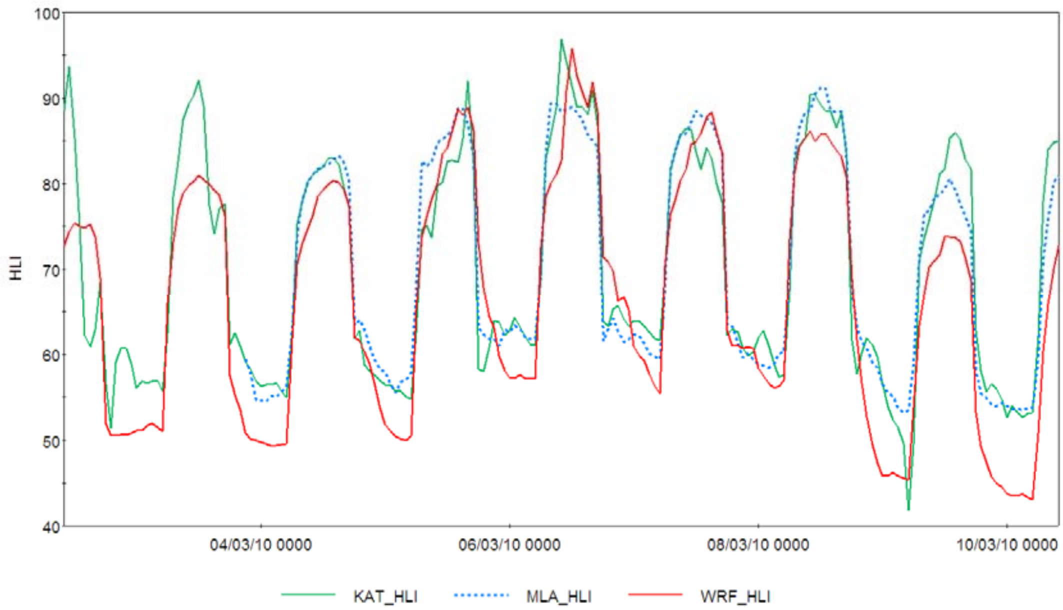

Figure F4 Heat Load Index (HLI) at Feedlot 2 calculated by MLA, KAT and WRF for the forecast assessment periods

Location: Feedlot 2	Period: February and March 2010	Data source: MLA,KAT and WRF	Units: HLI
Type: Time series		Prepared by: Andrew Vernon	Date: July 2010

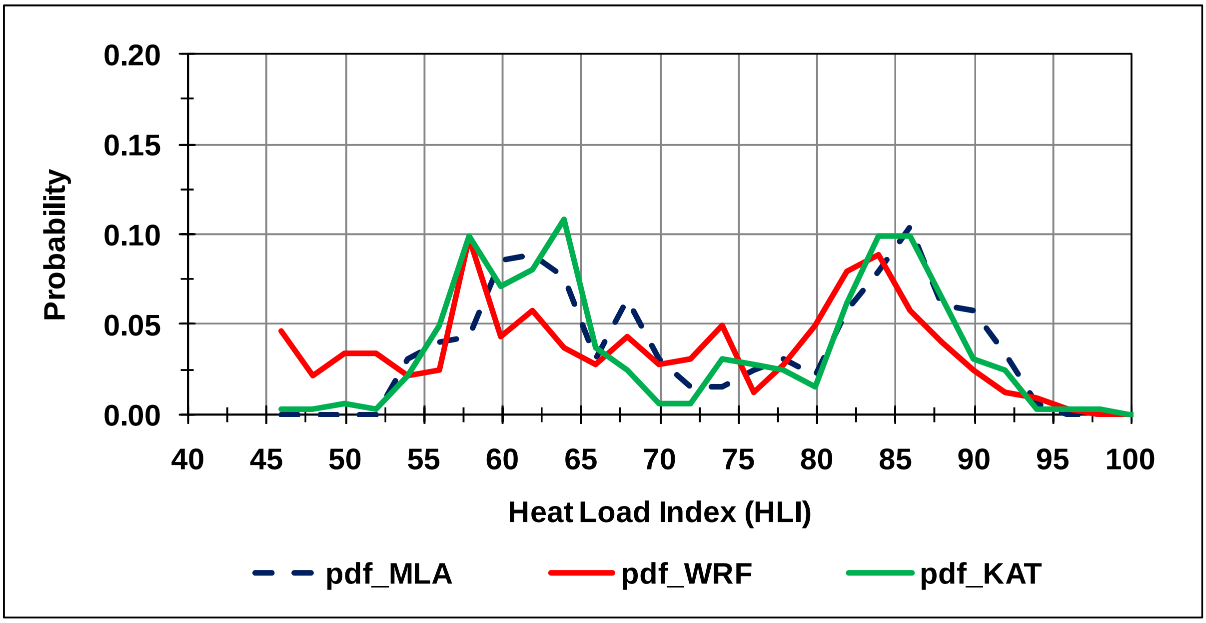

Figure F5 Heat Load Index (HLI) probability density function (pdf) at Feedlot 2 for MLA, KAT and WRF

Location: Feedlot 2	Period: February and March 2010	Data source: MLA,KAT and WRF	Units: probability
Type: pdf plot		Prepared by: Andrew Vernon	Date: July 2010

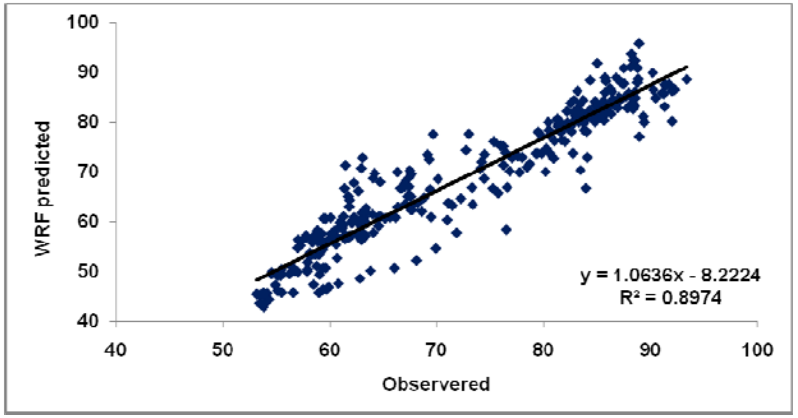

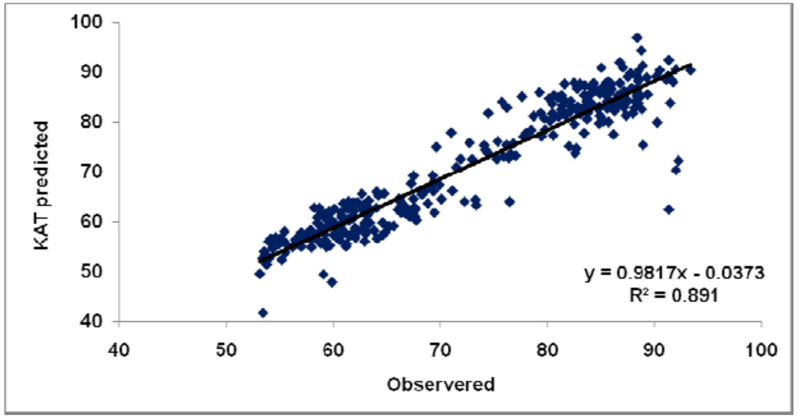

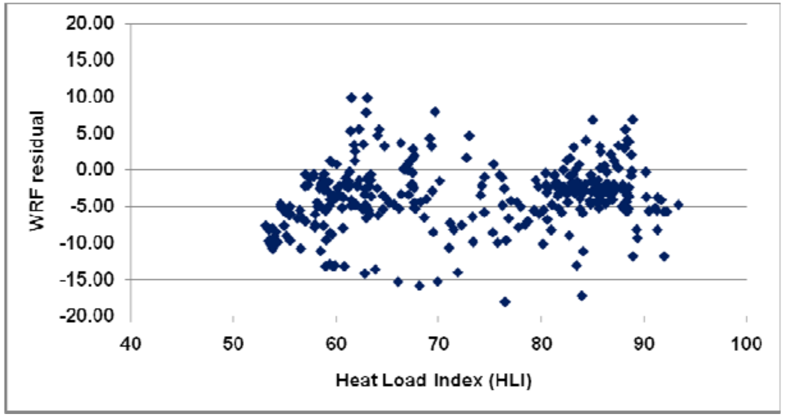

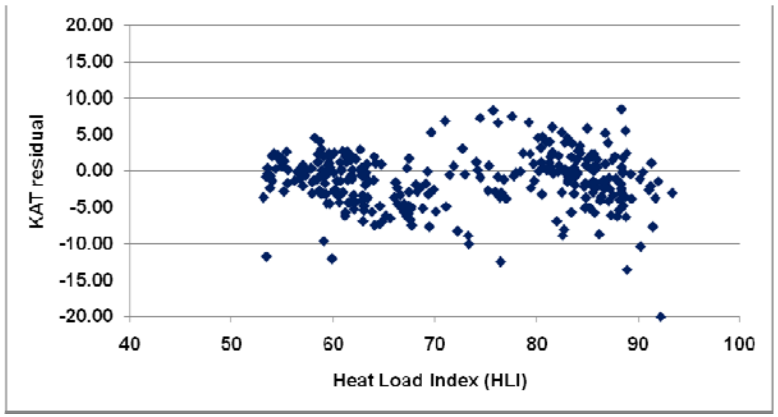

Figure F6 Regression and residual plots of HLI from KAT and WRF predictions at Feedlot 2

Type:	Data source:	Prepared by:	Date:
Regression and residuals charts	KAT and WRF	Andrew Vernon	July 2010

FEEDLOT 3 STATISTICS AND FIGURES

Table F5 Summary statistics of meteorology and heat load index measured onsite and modelled in WRF and KAT for Feedlot 3

Parameter	Average	Standard Deviation	Minimum	Maximum
MLA_HLI	70.80	13.29	47.48	95.47
WRF_HLI	64.54	13.46	42.55	91.92
KAT_HLI	69.88	13.42	43.48	93.10
MLA HLI	24.42	5.05	14.05	36.10
WRF HLI	22.18	4.01	11.95	31.05
KAT HLI	22.51	4.43	13.44	31.62
MLA Temperature (°C)	62.35	22.15	21.00	108.50
WRF Temperature (°C)	66.03	16.98	30.07	97.44
KAT Temperature (°C)	75.48	18.42	36.51	100.00
MLA Relative Humidity (%)	1.44	1.09	0.00	5.53
WRF Relative Humidity (%)	3.93	1.73	0.23	9.09
KAT Relative Humidity (%)	2.41	1.81	0.10	13.76

Table F6 Performance statistics of meteorology and heat load index measured onsite and modelled in WRF and KAT for Feedlot 3

Parameter	Intercept	Slope	r^2	RMSE	$RMSE_s$	$RMSE_u$	IOA	RCOR	ME
WRF HLI	-4.20	0.97	0.92	7.35	6.27	3.83	0.93	0.96	-6.26
KAT HLI	1.91	0.96	0.90	4.29	1.06	4.15	0.97	0.95	-0.91
WRF Temperature (°C)	4.11	0.74	0.87	2.98	2.60	1.46	0.90	0.93	-2.24
KAT Temperature (°C)	4.08	0.75	0.74	3.19	2.27	2.25	0.89	0.86	-1.90
WRF Relative Humidity (%)	28.16	0.61	0.63	13.99	9.43	10.34	0.86	0.79	3.69
KAT Relative Humidity (%)	39.34	0.58	0.49	20.80	16.09	13.19	0.75	0.70	13.13
WRF Wind speed (m/s)	2.60	0.92	0.34	2.86	2.49	1.40	0.48	0.59	2.49
KAT Wind speed (m/s)	1.05	0.94	0.32	1.77	0.97	1.48	0.64	0.57	0.96

a) February Forecast

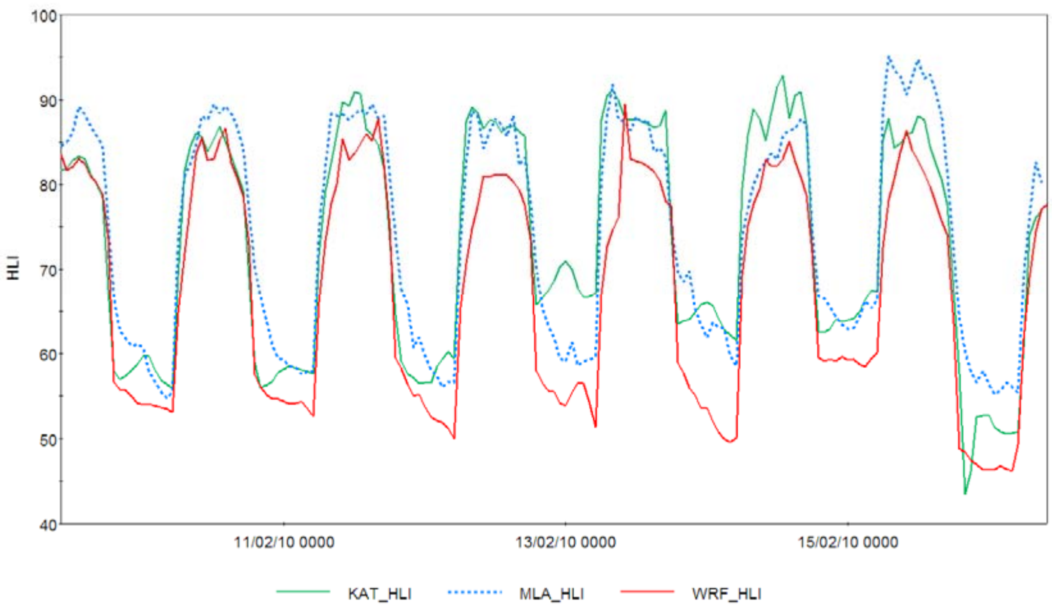

b) March Forecast

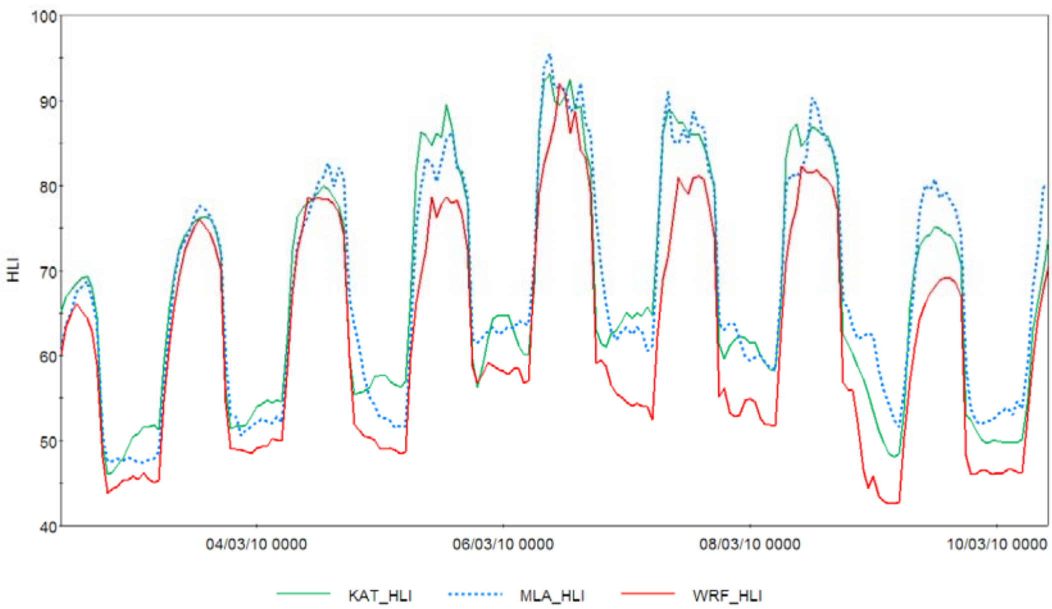

Figure F7 Heat Load Index (HLI) at Feedlot 3 calculated by MLA, KAT and WRF for the forecast assessment periods

Location: Feedlot 3	Period: February and March 2010	Data source: MLA,KAT and WRF	Units: HLI
Type: Time series		Prepared by: Andrew Vernon	Date: July 2010

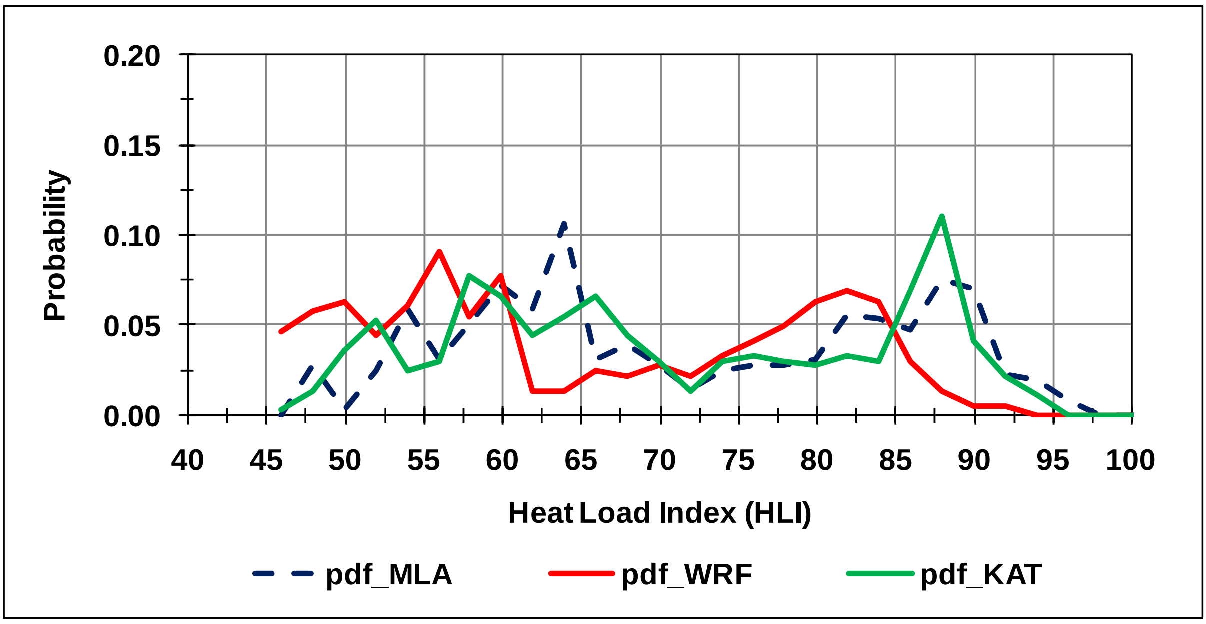

Figure F8	Heat Load Index (HLI) probability density function (pdf) at Feedlot 3 for MLA, KAT and WRF		
Location: Feedlot 3	Period: February and March 2010	Data source: MLA,KAT and WRF	Units: probability
Type: pdf plot		Prepared by: Andrew Vernon	Date: July 2010

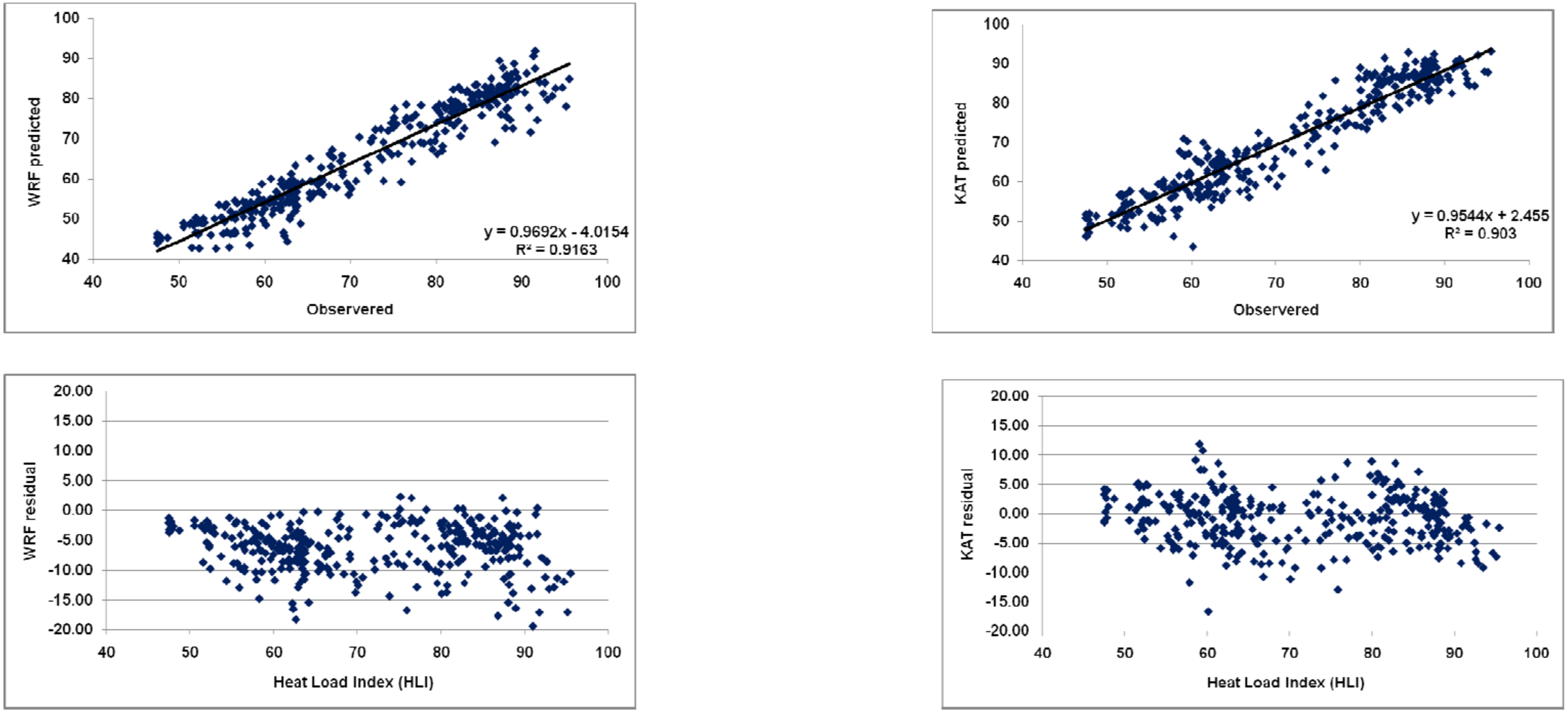

Figure F9 Regression and residual plots of HLI from KAT and WRF predictions at Feedlot 3

Type: Regression and residuals charts	Data source: KAT and WRF	Prepared by: Andrew Vernon	Date: July 2010

FEEDLOT 4 STATISTICS AND FIGURES

Table F7 Summary statistics of meteorology and heat load index measured onsite and modelled in WRF and KAT for Feedlot 4

Parameter	Average	Standard Deviation	Minimum	Maximum
MLA_HLI	65.57	13.29	41.63	100.76
WRF_HLI	65.56	13.88	38.14	90.83
KAT_HLI	63.97	15.03	32.98	87.02
MLA HLI	23.28	4.96	10.95	37.05
WRF HLI	23.94	4.39	12.56	36.06
KAT HLI	23.75	5.25	8.09	35.50
MLA Temperature (°C)	57.73	21.16	17.00	101.00
WRF Temperature (°C)	57.98	17.69	19.79	95.85
KAT Temperature (°C)	63.44	18.32	27.32	100.00
MLA Relative Humidity (%)	2.45	1.15	0.35	8.07
WRF Relative Humidity (%)	3.97	1.76	0.22	8.80
KAT Relative Humidity (%)	7.48	2.78	2.30	14.92

Table F8 Performance statistics of meteorology and heat load index measured onsite and modelled in WRF and KAT for Feedlot 4

Parameter	Intercept	Slope	r^2	RMSE	$RMSE_s$	$RMSE_u$	IOA	RCOR	ME
WRF HLI	-0.41	1.01	0.93	3.74	0.08	3.74	0.98	0.96	0.00
KAT HLI	-5.55	1.06	0.88	5.51	1.79	5.21	0.96	0.94	-1.60
WRF Temperature (°C)	5.36	0.80	0.82	2.23	1.20	1.88	0.94	0.90	0.65
KAT Temperature (°C)	2.94	0.89	0.71	2.89	0.71	2.80	0.92	0.85	0.47
WRF Relative Humidity (%)	20.62	0.65	0.60	13.45	7.46	11.19	0.87	0.77	0.25
KAT Relative Humidity (%)	26.29	0.64	0.55	15.46	9.45	12.23	0.84	0.74	5.71
WRF Wind speed (m/s)	2.51	0.60	0.15	2.27	1.59	1.62	0.51	0.39	1.52
KAT Wind speed (m/s)	4.69	1.14	0.22	5.59	5.03	2.44	0.28	0.47	5.03

a) February Forecast

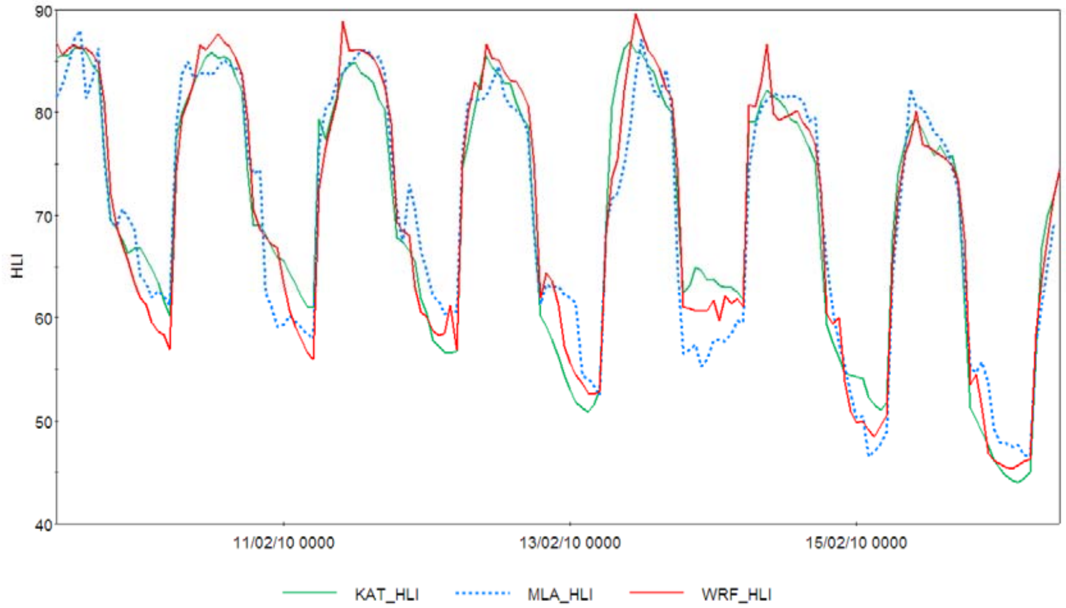

b) March Forecast

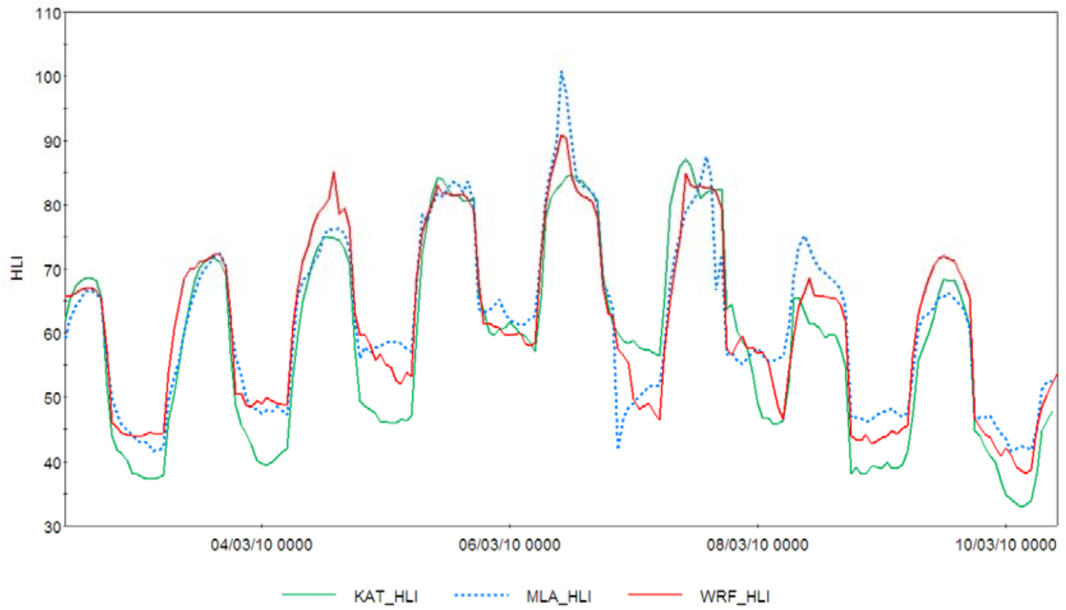

Figure F10 Heat Load Index (HLI) at Feedlot 4 calculated by MLA, KAT and WRF for the forecast assessment periods

Location: Feedlot 4	Period: February and March 2010	Data source: MLA,KAT and WRF	Units: HLI
Type: Timeseries		Prepared by: Andrew Vernon	Date: July 2010

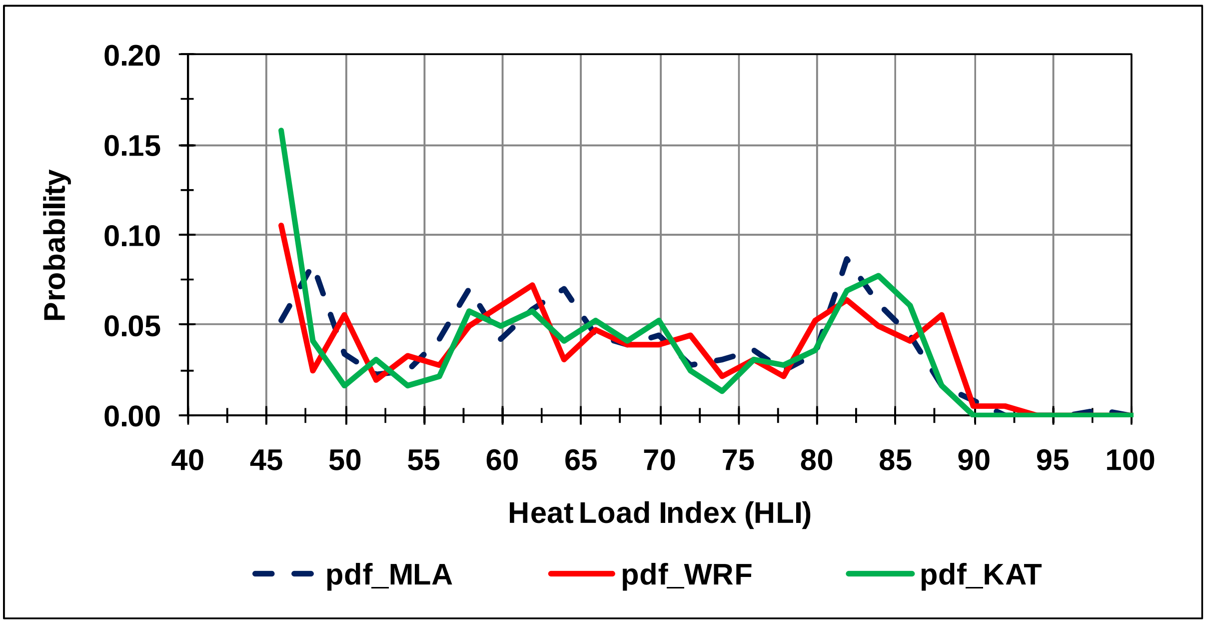

Figure F11	Heat Load Index (HLI) probability density funtion (pdf) at Feedlot 4 for MLA, KAT and WRF

Location: Feedlot 4	Period: February and March 2010	Data source: MLA,KAT and WRF	Units: probability
Type: pdf plot		Prepared by: Andrew Vernon	Date: July 2010

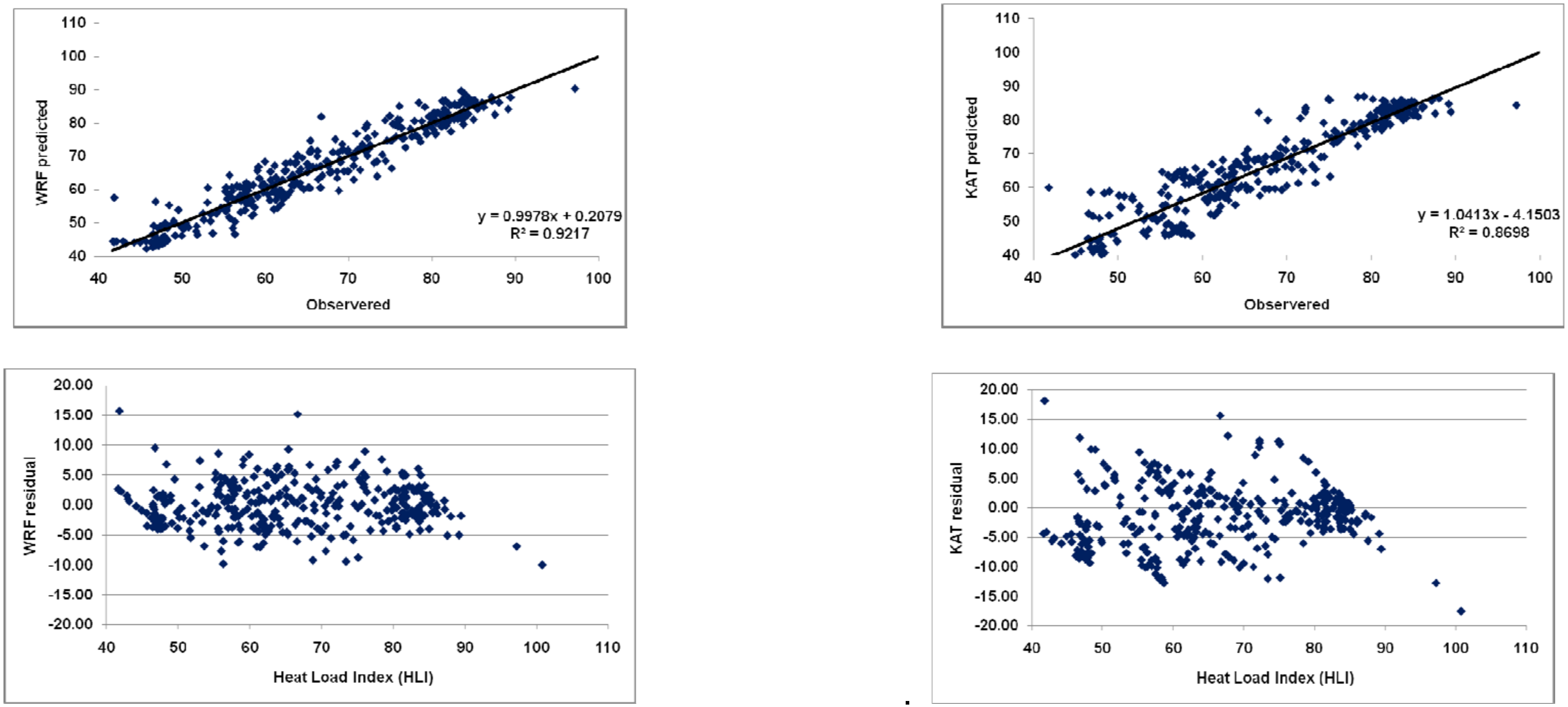

Figure F12 Regression and residual plots of HLI from KAT and WRF predictions at Feedlot 4

Type:	Data source:	Prepared by:	Date:
Regression and residuals charts	KAT and WRF	Andrew Vernon	July 2010

FEEDLOT 5 STATISTICS AND FIGURES

Table F9 Summary statistics of meteorology and heat load index measured onsite and modelled in WRF and KAT for Feedlot 5

Parameter	Average	Standard Deviation	Minimum	Maximum
MLA_HLI	64.55	13.23	41.73	89.67
WRF_HLI	65.18	13.51	41.58	94.96
KAT_HLI	66.22	13.85	42.90	92.95
MLA HLI	23.29	5.67	8.10	38.20
WRF HLI	23.62	4.93	14.90	36.28
KAT HLI	22.91	5.18	13.70	34.94
MLA Temperature (°C)	54.63	18.94	20.00	88.00
WRF Temperature (°C)	57.43	18.09	21.54	93.07
KAT Temperature (°C)	63.57	21.37	23.24	100.00
MLA Relative Humidity (%)	2.95	1.54	0.14	9.39
WRF Relative Humidity (%)	3.88	1.84	0.11	8.64
KAT Relative Humidity (%)	3.38	1.70	0.37	8.68

Table F10 Performance statistics of meteorology and heat load index measured onsite and modelled in WRF and KAT for Feedlot 5

Parameter	Intercept	Slope	r^2	RMSE	$RMSE_s$	$RMSE_u$	IOA	RCOR	ME
WRF HLI	1.13	0.99	0.94	3.27	0.63	3.21	0.98	0.97	0.62
KAT HLI	1.86	1.00	0.91	4.54	1.67	4.22	0.97	0.95	1.67
WRF Temperature (°C)	5.07	0.80	0.84	2.32	1.20	1.98	0.95	0.92	0.32
KAT Temperature (°C)	3.97	0.81	0.79	2.61	1.12	2.36	0.94	0.89	-0.38
WRF Relative Humidity (%)	13.92	0.80	0.70	11.04	4.76	9.96	0.91	0.83	2.80
KAT Relative Humidity (%)	10.66	0.97	0.74	14.15	8.96	10.95	0.88	0.86	8.94
WRF Wind speed (m/s)	1.69	0.74	0.39	1.76	1.01	1.44	0.73	0.62	0.93
KAT Wind speed (m/s)	1.81	0.53	0.23	1.71	0.84	1.48	0.69	0.48	0.43

a) February Forecast

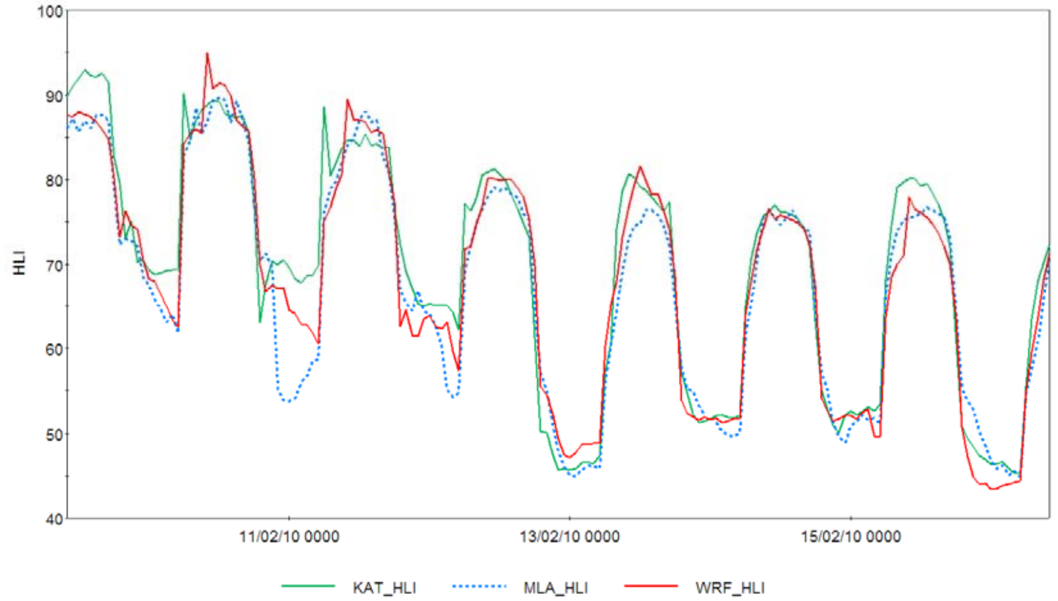

b) March Forecast

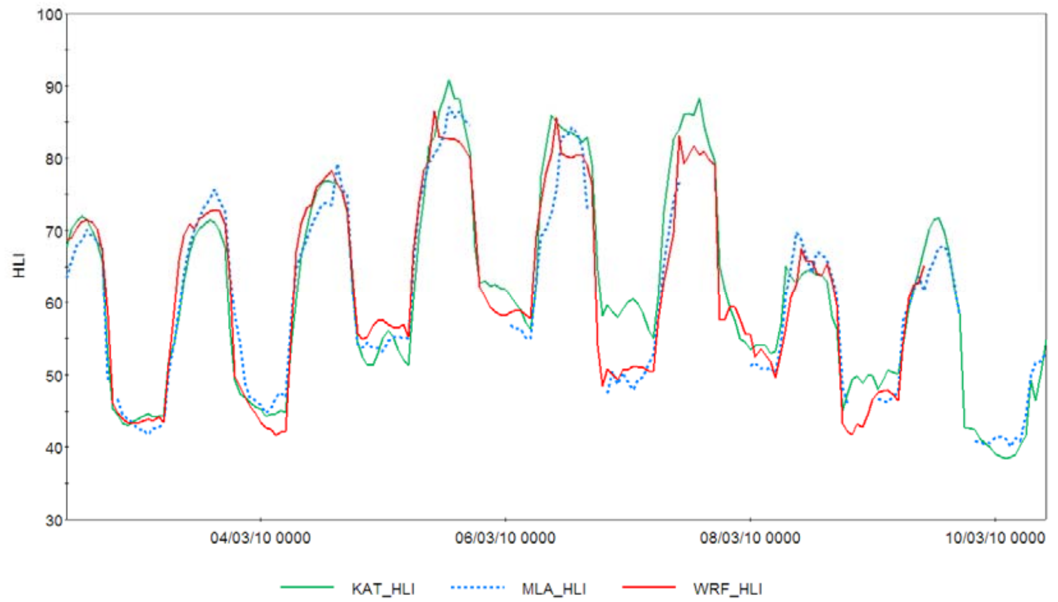

Figure F13 Heat Load Index (HLI) at Feedlot 5 calculated by MLA, KAT and WRF for the forecast assessment periods

Location: Feedlot 5	Period: February and March 2010	Data source: MLA,KAT and WRF	Units: HLI
Type: Time series		Prepared by: Andrew Vernon	Date: July 2010

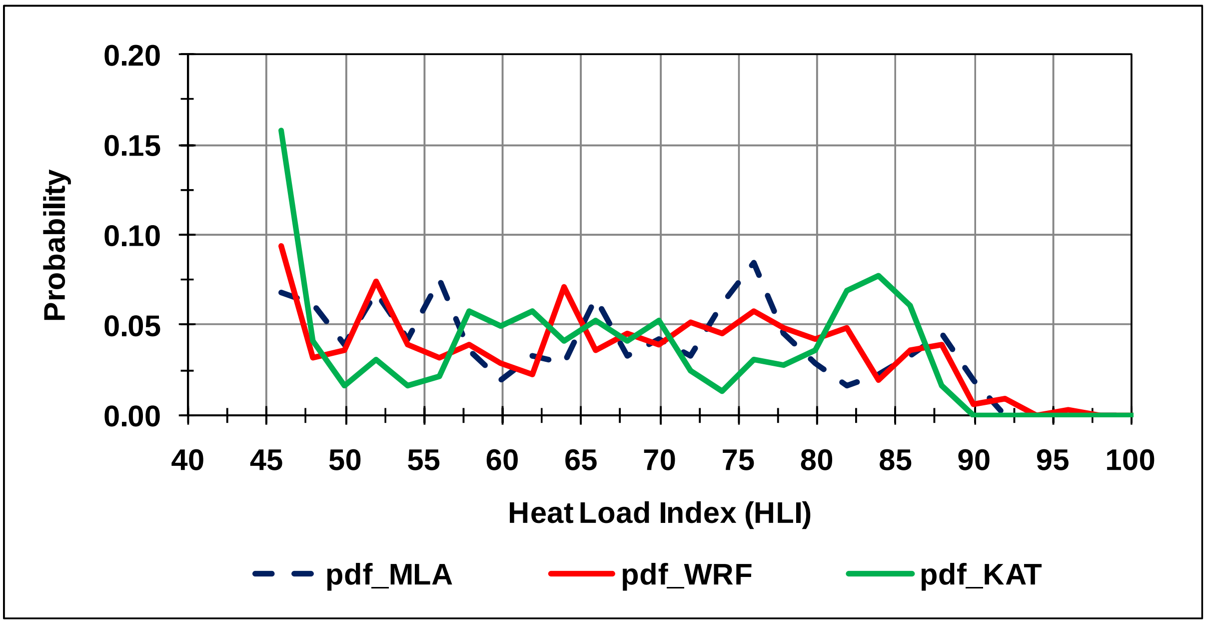

Figure F14 Heat Load Index (HLI) probability density function (pdf) at Feedlot 5 for MLA, KAT and WRF

Location: Feedlot 5	Period: February and March 2010	Data source: MLA,KAT and WRF	Units: probability
Type: pdf plot		Prepared by: Andrew Vernon	Date: July 2010

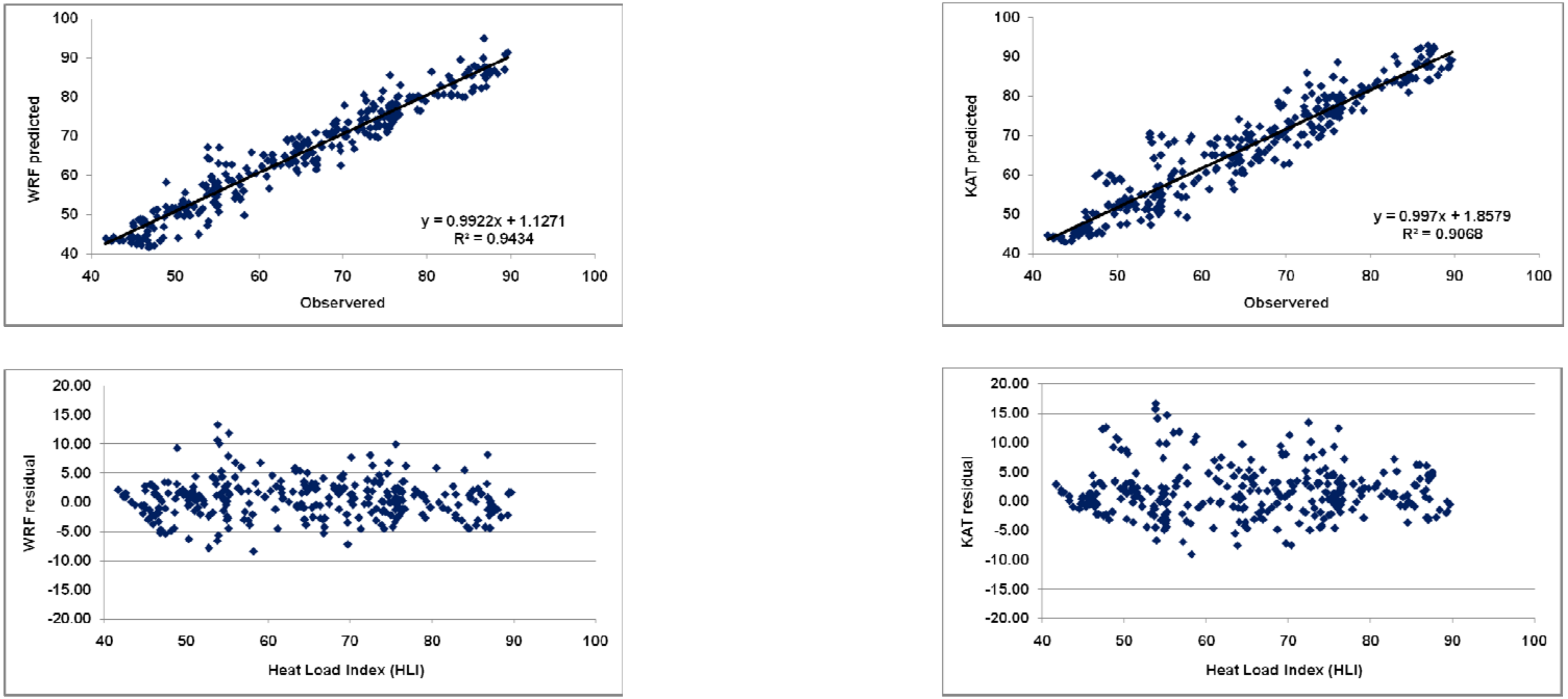

Figure F15 Regression and residual plots of HLI from KAT and WRF predictions at Feedlot 5

Type: Regression and residuals charts	Data source: KAT and WRF	Prepared by: Andrew Vernon	Date: July 2010

FEEDLOT 6 STATISTICS AND FIGURES

Table F11 Summary statistics of meteorology and heat load index measured onsite and modelled in WRF and KAT for Feedlot 6

Parameter	Average	Standard Deviation	Minimum	Maximum
MLA_HLI	65.77	14.91	39.47	104.36
WRF_HLI	62.01	13.81	36.92	91.81
KAT_HLI	63.61	14.30	35.97	94.43
MLA HLI	21.21	5.85	9.82	37.50
WRF HLI	21.29	5.42	9.78	33.79
KAT HLI	22.36	6.29	9.71	37.94
MLA Temperature (°C)	66.43	22.69	22.00	96.67
WRF Temperature (°C)	63.83	18.48	24.93	94.27
KAT Temperature (°C)	64.54	21.97	26.54	100.82
MLA Relative Humidity (%)	2.73	1.84	0.00	7.69
WRF Relative Humidity (%)	3.96	1.91	0.19	9.62
KAT Relative Humidity (%)	6.13	2.84	0.33	18.67

Table F12 Performance statistics of meteorology and heat load index measured onsite and modelled in WRF and KAT for Feedlot 6

Parameter	Intercept	Slope	r^2	RMSE	$RMSE_s$	$RMSE_u$	IOA	RCOR	ME
WRF HLI	6.03	0.85	0.84	6.98	4.37	5.44	0.94	0.92	-3.77
KAT HLI	8.07	0.84	0.77	7.48	3.17	6.78	0.93	0.88	-2.16
WRF Temperature (°C)	2.85	0.87	0.88	2.01	0.77	1.86	0.97	0.94	0.08
KAT Temperature (°C)	0.61	1.03	0.91	2.20	1.16	1.87	0.97	0.95	1.15
WRF Relative Humidity (%)	18.38	0.68	0.71	12.58	7.61	10.01	0.90	0.84	-2.60
KAT Relative Humidity (%)	5.78	0.88	0.83	9.48	3.23	8.92	0.95	0.91	-1.89
WRF Wind speed (m/s)	2.85	0.41	0.15	2.40	1.64	1.75	0.59	0.39	1.23
KAT Wind speed (m/s)	4.43	0.62	0.16	4.33	3.47	2.60	0.44	0.40	3.40

a) February Forecast

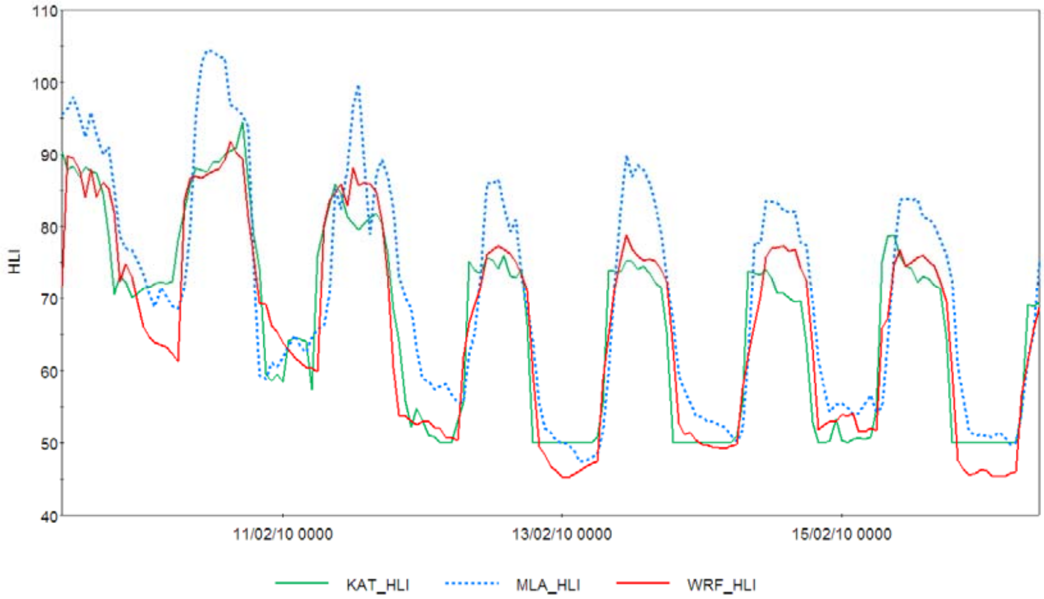

b) March Forecast

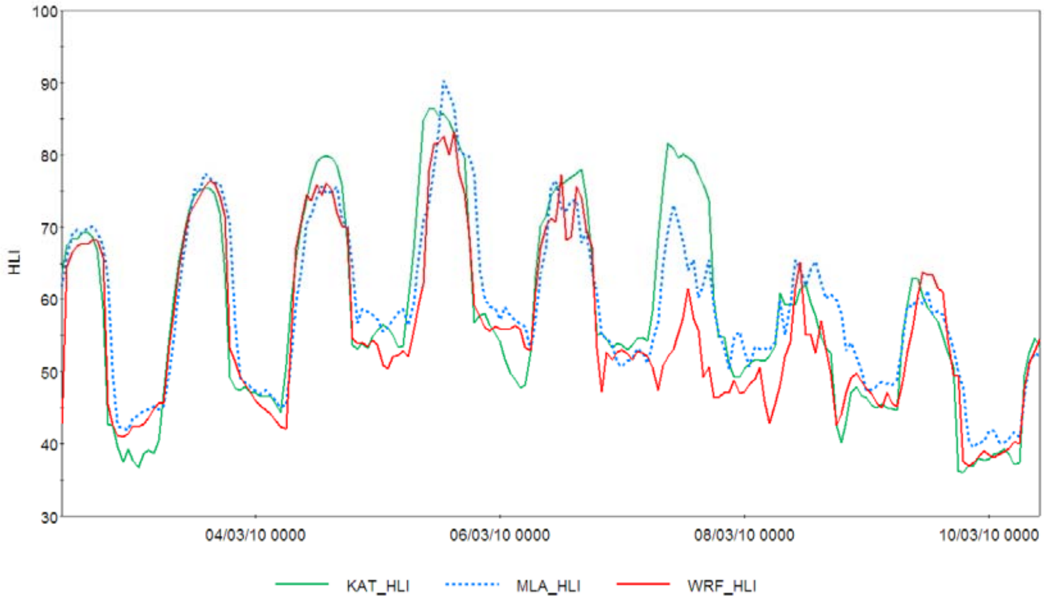

Figure F16 Heat Load Index (HLI) at Feedlot 6 calculated by MLA, KAT and WRF for the forecast assessment periods

Location: Feedlot 6	Period: February and March 2010	Data source: MLA,KAT and WRF	Units: HLI
Type: Timeseries		Prepared by: Andrew Vernon	Date: July 2010

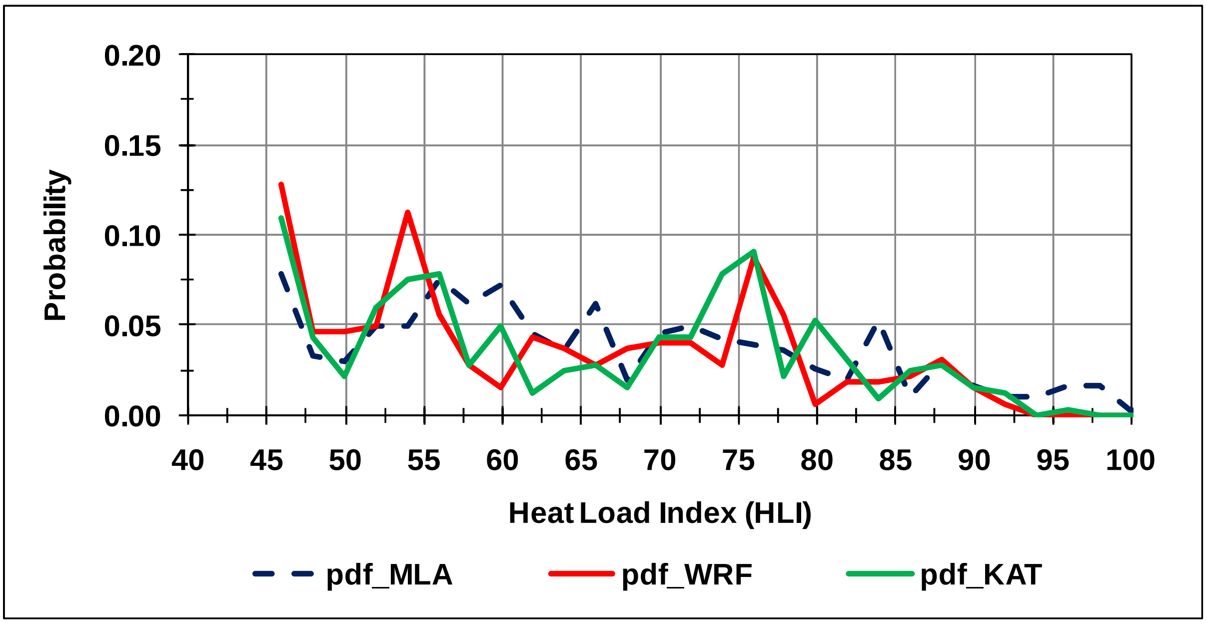

Figure F17	Heat Load Index (HLI) probability density function (pdf) at Feedlot 6 for MLA, KAT and WRF

Location: Feedlot 6	Period: February and March 2010	Data source: MLA,KAT and WRF	Units: probability
Type: pdf plot		Prepared by: Andrew Vernon	Date: July 2010

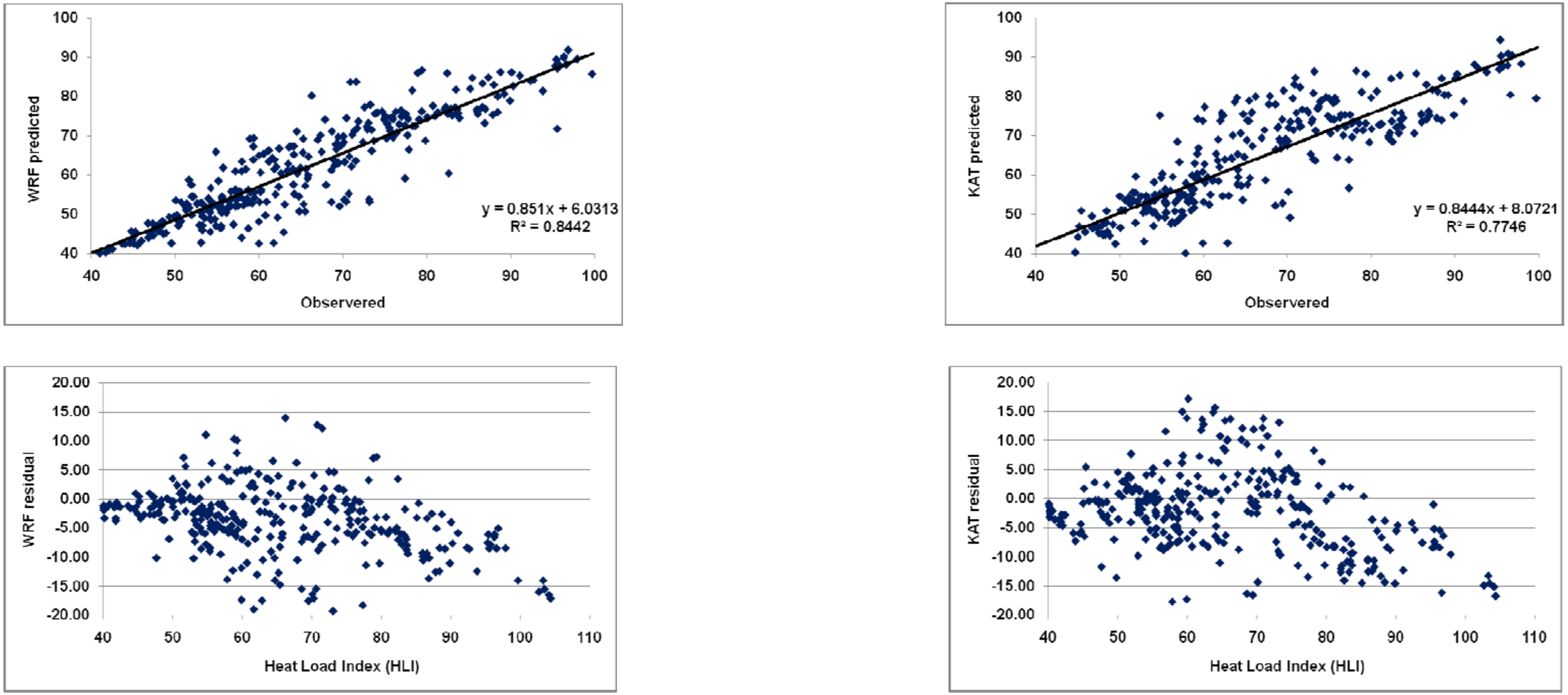

Figure F18 Regression and residual plots of HLI from KAT and WRF predictions at Feedlot 6

Type:	Data source:	Prepared by:	Date:
Regression and residuals charts	KAT and WRF	Andrew Vernon	July 2010